Received: 31 October 2023 | Revised: 23 May 2024 | Accepted: 14 June 2024

DOI: 10.1111/pce.15018

ORIGINAL ARTICLE

Plant, Cell & Environment PC&E WILEY

Dynamic changes in mRNA nucleocytoplasmic localization in the nitrate response of Arabidopsis roots

Alejandro Fonseca[1,2,3,4] | Eleodoro Riveras[1,2,3] | Tomás C. Moyano[1,2,3,5] | José M. Alvarez[1,5] | Stefanie Rosa[4] | Rodrigo A. Gutiérrez[1,2,3]

[1]Millennium Institute for Integrative Biology (iBio), Santiago, Chile

[2]Center for Genome Regulation, Millennium Institute Center for Genome Regulation (CRG), Santiago, Chile

[3]Departamento de Genética Molecular y Microbiología, Facultad de Ciencias Biológicas, Pontificia Universidad Católica de Chile, Santiago, Chile

[4]Department of Plant Biology, Swedish University of Agricultural Sciences (SLU), Uppsala, Sweden

[5]Centro de Biotecnología Vegetal, Facultad de Ciencias de la Vida, Universidad Andrés Bello, Santiago, Chile

Correspondence
Rodrigo A. Gutiérrez, Millennium Institute for Integrative Biology (iBio), Santiago, Chile.
Email: rgutierrez@bio.puc.cl

Funding information
ANID FONDECYT, Grant/Award Numbers: 1210389, 3220801, 11230913, 1180759; Knut och Alice Wallenbergs Stiftelse, Grant/Award Number: 2019-0206; Vetenskapsrådet, Grant/Award Number: 2018-04101; Center for Genome Regulation, Grant/Award Number: ICN2021_044; Millennium Institute for Integrative Biology (iBio), Grant/Award Number: ICN17_022; NSF Plant Genome Grant NSF-PGRP, Grant/Award Number: IOS-1840761; CONICYT Beca Doctorado Nacional, Grant/Award Number: 21161516

Abstract

Nitrate is a nutrient and signal that regulates gene expression. The nitrate response has been extensively characterized at the organism, organ, and cell-type-specific levels, but intracellular mRNA dynamics remain unexplored. To characterize nuclear and cytoplasmic transcriptome dynamics in response to nitrate, we performed a time-course expression analysis after nitrate treatment in isolated nuclei, cytoplasm, and whole roots. We identified 402 differentially localized transcripts (DLTs) in response to nitrate treatment. Induced DLT genes showed rapid and transient recruitment of the RNA polymerase II, together with an increase in the mRNA turnover rates. DLTs code for genes involved in metabolic processes, localization, and response to stimulus indicating DLTs include genes with relevant functions for the nitrate response that have not been previously identified. Using single-molecule RNA FISH, we observed early nuclear accumulation of the *NITRATE REDUCTASE 1* (*NIA1*) transcripts in their transcription sites. We found that transcription of *NIA1*, a gene showing delayed cytoplasmic accumulation, is rapidly and transiently activated; however, its transcripts become unstable when they reach the cytoplasm. Our study reveals the dynamic localization of mRNAs between the nucleus and cytoplasm as an emerging feature in the temporal control of gene expression in response to nitrate treatment in Arabidopsis roots.

KEYWORDS
gene expression regulation, nitrate, RNA dynamics, subcellular localization

1 | INTRODUCTION

Nitrogen (N) is an essential macronutrient whose availability limits plant growth and development (Alvarez et al., 2021; Andrews et al., 2013; Araus et al., 2020; Fredes et al., 2019; Gutiérrez, 2012; Vidal et al., 2020). Nitrate is the most abundant source of N in agricultural soils (Owen & Jones, 2001). Nitrate acts as a signalling molecule (Scheible et al., 1997; Wang et al., 2004) that initiates a signal transduction cascade (Undurraga et al., 2017; Vidal et al., 2020). The dual-affinity transceptor NPF6.3/NRT1.1 was the first nitrate sensor described (Ho et al., 2009). In addition, NLP7 transcription factors (TFs) have been also proposed as intracellular nitrate sensors (Liu et al., 2022). Different regulatory factors, at the local and systemic level, orchestrate downstream responses affecting nutrient metabolism and a series of developmental processes associated with root development (Alvarez et al., 2014; Canales et al., 2017;

Forde & Walch-Liu, 2009; Gruber et al., 2013; O'Brien et al., 2016; Vidal et al., 2010), shoot development (Landrein et al., 2018; Moreno et al., 2020; Poitout et al., 2018; Rahayu et al., 2005), seed dormancy (Alboresi et al., 2005; Yan et al., 2016), and flowering time (Castro Marín et al., 2011; Gras et al., 2018). In addition to the NRT1.1 transceptor, critical components in the nitrate signalling pathway include CIPK23 kinase (Liu & Tsay, 2003), calcium as a second messenger (Riveras et al., 2015), and a myriad of TFs controlling transcriptional responses (reviewed in (Vidal et al., 2020)).

In eukaryotic cells, mRNA synthesis and processing occur within the nucleus, while translation mainly happens in the cytoplasm (Martin & Koonin, 2006). The sequencing of RNA from cellular fractions of different eukaryotic species showed that transcripts are asymmetrically distributed between the nucleus and cytoplasm (Bahar Halpern et al., 2015; Barthelson et al., 2007; Battich et al., 2015; Benoit Bouvrette et al., 2018; Chen & Van Steensel, 2017; Djebali et al., 2012; Pastro et al., 2017; Reynoso et al., 2019; Solnestam et al., 2012; Abdelmoez et al., 2018; de Leone et al., 2020; Kim et al., 2017; Lee & Bailey-Serres, 2019; Palovaara & Weijers, 2019; Price et al., 2020). Controlling mRNA localization allows the cell to fine-tune gene expression according to environmental and cellular requirements (Chen & Van Steensel, 2017; de Leone et al., 2020; Lee & Bailey-Serres, 2019; Parry, 2015; Wickramasinghe & Laskey, 2015; Yang et al., 2017). The nucleocytoplasmic dynamic of transcripts is mostly determined by synthesis, export, and decay factors (Bahar Halpern et al., 2015; Hansen et al., 2018). Synthesis and decay rates have been quantified at the genome-wide level in yeast (Eser et al., 2014; Miller et al., 2011; Sun et al., 2012), mice (Jovanovic et al., 2015; Rabani et al., 2014; Schwanhäusser et al., 2011; Tippmann et al., 2012), flies (Chen & Van Steensel, 2017), and plants (Gutiérrez et al., 2002; Sorenson et al., 2018; Szabo et al., 2020). These results indicate that synthesis and decay rates contribute to mRNA steady-state levels differently potentially resulting in changes in the RNA distribution, allowing for sophisticated regulation of gene expression (Wickramasinghe & Laskey, 2015).

In plants, the nuclear export-machinery components are more diverse than in yeast or animals (Pfaff et al., 2018; Yelina et al., 2010), suggesting that their ability to regulate mRNA localization in response to a stimulus is more versatile (Ehrnsberger et al., 2019). Some studies have shown that subsets of mRNAs display particular nucleocytoplasmic distributions during different plant processes, such as cell cycle control (Yang et al., 2017), ethylene signalling (Chen et al., 2019), RNA-directed DNA methylation (Choudury et al., 2019), and stress response (Yeap et al., 2019). However, the mRNA nucleocytoplasmic dynamics at the genome-wide level have only been described in response to bacterial, hypoxia, and flooding stresses (de Leone et al., 2020; Lee & Bailey-Serres, 2019; Reynoso et al., 2019). Genome-wide changes in gene expression in response to nitrate treatments have been thoroughly characterized in several studies (Alvarez et al., 2014, 2019; Gaudinier et al., 2018; Gifford et al., 2008; Gutiérrez et al., 2007; Hu et al., 2009; Krouk et al., 2009, 2010; Moreno et al., 2020; Patterson et al., 2010; Ruffel et al., 2011; Varala et al., 2018; Vidal et al., 2013; Walker et al., 2017; Wang et al., 2003, 2004, 2007; Swift et al., 2020). However, we lack understanding of the importance of mRNA nucleocytoplasmic dynamics in response to changes in nutrient availability.

In this work, we aimed to characterize the nucleocytoplasmic dynamics of mRNAs in response to nitrate treatment. We used RNA-seq analysis from nuclear, cytoplasmic, and total fractions to identify differentially localized transcripts (DLTs) in response to nitrate. Integrated analysis of our genome-wide data showed that DLTs have significant synthesis and decay rate changes, indicating these mRNAs are rapidly replaced during the nitrate response. Our results reveal that the nucleocytoplasmic distribution of mRNA can contribute to fine-tune dynamic gene expression changes in response to nitrate treatments in plants. This layer of gene expression control contributes to the exquisite ability of plants to adapt to nutritional changes in their environment.

2 | RESULTS

2.1 | Identification of differentially expressed genes in response to nitrate treatment in nuclear and cytoplasmic subcellular fractions

To characterize the distribution of messenger RNAs in the nucleus and cytoplasm of Arabidopsis root cells in response to nitrate treatment, we conducted a time-course experiment. This involved subjecting roots to nitrate treatment for 20, 60, and 120 min, followed by mRNA sequencing of nuclear, cytoplasmic, and whole-cells fractions. Cell fractions were separated through differential centrifugation as described in Section 4 (Figure 1a). To validate our cellular fractionation protocol, we evaluated the integrity and purity of the extracted nuclei by DAPI staining and fluorescence microscopy (Supporting Information S2: Figure 1A). In addition, we corroborated the purity of our subcellular fractions by immunoblot, using antibodies against HISTONE 3 (H3) as a nuclear marker, and to conserved regions of ACTIN1/2/3/4/5/7/8/11/12 (ACT) as cytoplasmic markers (Dalmadi et al., 2019) (Figure 1b). All our control experiments indicated the subcellular fractions have been correctly isolated.

We performed transcriptome sequencing from Poly(A) enriched RNA for each subcellular fraction. The sequencing data obtained was normalized using two approaches: (i) normalized by transcripts per million (TPM) to adjust transcript levels according to the total amount of sequenced RNA in each cellular fraction, and (ii) quantile normalization to rank the RNA levels within each fraction and reduce possible biases generated by technical differences in the fractionation protocol (Barthelson et al., 2007; Kim et al., 2017; Reynoso et al., 2019). To evaluate how the fractions and replicates clustered, we conducted principal component analysis (PCA) and correlation analysis. The results showed that samples are primarily separated by fractions, indicating that each has a distinct transcriptome (Supporting Information S2: Figure 1B), and the correlation analysis revealed

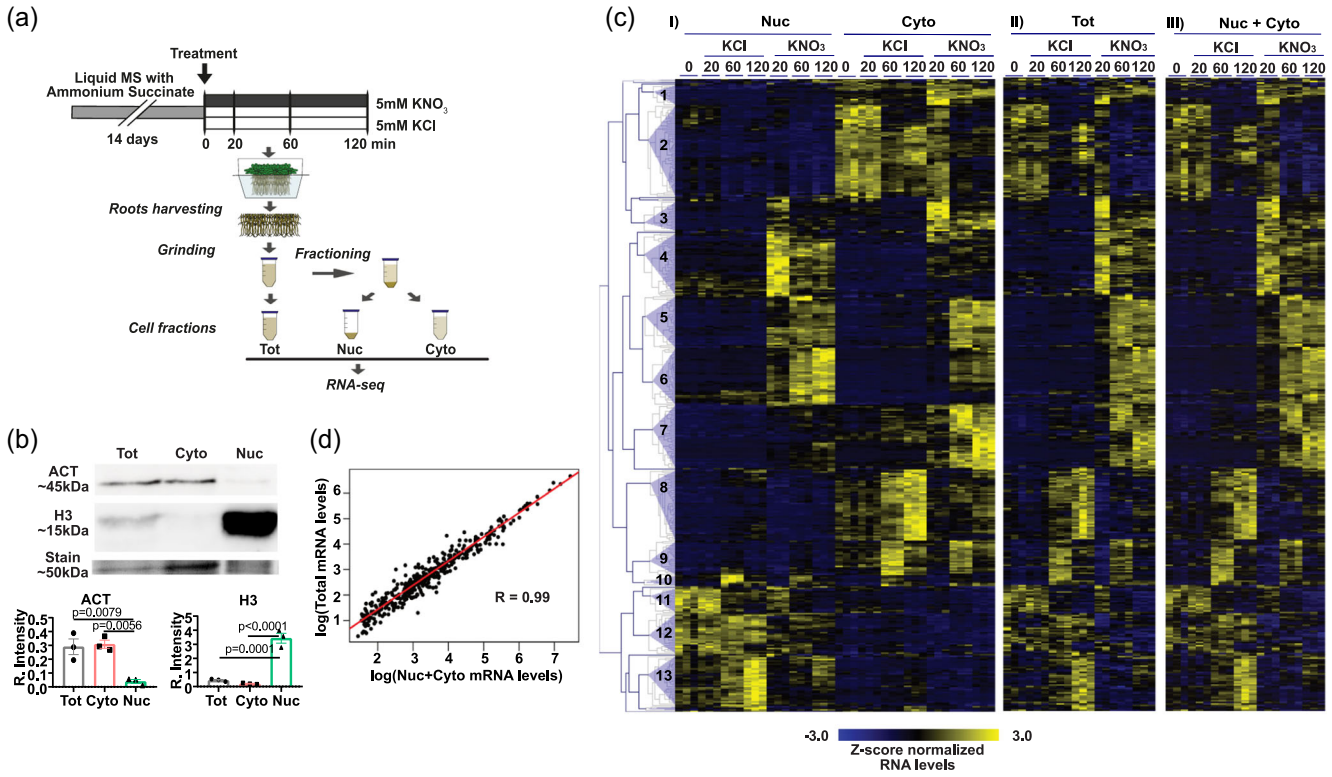

FIGURE 1 RNA-seq from cellular fractions identifies differentially localized transcripts (DLTs) in response to nitrate treatments. (a) Diagram describing the experimental design. Fourteen-day-old seedlings were treated with 5 mM KNO3 (or KCl as control). Roots were harvested at 0, 20, 60, and 120 min after the nutrient application. The tissue was ground and fractionated to perform RNA-seq from the total (Tot), nuclear (Nuc), and cytoplasmic (Cyto) fractions. (b) Immunoblot analysis to control fractioning efficiency. The nuclear marker HISTONE 3 (H3) and the cytoplasmic markers ACTIN1/2/3/4/5/7/8/11/12 (ACT) were evaluated in the total (Tot), nuclear (Nuc), and cytoplasmic (Cyto) fractions. A common band observed with Coomassie blue staining was included as a loading control. Plots to the bottom show the relative intensity (R. Intensity) of the immunodetected bands normalized by the Coomassie staining, three independent experiments were included. (c) Heatmaps with mRNA levels in cellular fractions for DLTs in response to nitrate treatments. Genes were hierarchically clustered using the correlation of mRNA levels in the nuclear (Nuc) and cytoplasmic (Cyto) fractions (panel I). mRNA levels in the total (Tot) fraction are shown in panel II. We calculated Nuclear+Cytoplasmic (Nuc+Cyto) RNA levels using data from each fraction, which are shown in panel III. Cluster numbers are indicated in the dendrogram to the left of the heatmap. Each column represents the mRNA levels for one replicate under each condition. Three independent experiments are included. (d) Scatter plot for comparing the mean mRNA levels of DLTs in the total fraction with the sum of the nuclear and cytoplasmic mRNA levels. The Pearson correlation (R) is indicated.

that replicates clustered together (Supporting Information S2: Figure 1C). As an additional control, we compared our normalized RNA levels to previously reported nuclear- or PolyA-enriched mRNA data reported for Arabidopsis (de Leone et al., 2020; Lee & Bailey-Serres, 2019) (Supporting Information S2: Figure 2). We observed a similar pattern in our subcellular fractions as compared with previously reported data. These results show expected differences between nuclear and cytoplasmic fractions, indicating that RNA enrichment in our subcellular fractions is comparable with previously published studies.

To identify differentially expressed genes in response to nitrate treatment in each subcellular fraction, we performed a two-way analysis of variance (ANOVA) with a false-discovery rate (FDR) of 0.01. We identified a total of 6006 genes in the whole cells, 2634 genes in the nuclear fraction, and 3482 genes in the cytoplasmic fraction that showed differential expression following nitrate treatments (Supporting Information S2: Figure 3A, Supporting Information S3: Data Set 1). To compare global gene expressions between subcellular fractions in response to nitrate treatments, we performed a correlation analysis of nitrate-responsive genes in nuclear, cytoplasmic and whole cell samples (Supporting Information S2: Figure 3B). Our results indicate that global gene expression patterns in response to nitrate treatments are largely congruent for total, cytoplasmic, and nuclear RNA samples. A total of 1183 genes were exclusively regulated in the subcellular fractions in response to the nitrate treatments (Supporting Information S2: Figure 4, Supporting Information S3: Data Set 1). This result indicates that subcellular fractions provide complementary information to the analysis of total fraction in response to nitrate treatment. In addition, we detected 418 (260 only in the cytoplasmic fraction, 121 only in the nuclear fraction, and 37 shared) new differentially expressed genes in response to nitrate treatment that had not been reported previously (Alvarez et al., 2019; Canales et al., 2014; Krouk et al., 2010; Varala et al., 2018) and are not identified in our total fraction (Supporting

Information S2: Figure 5, Supporting Information S4: Data Set 2). These genes represent new components of the nitrate response and could contribute to the plant adaptation to changes in N availability. Overall, these results revealed that nucleocytoplasmic distributions of mRNA may play an underappreciated role in plants' response to nitrate treatment.

2.2 | DLTs in response to nitrate treatments

To identify DLTs in response to nitrate treatment, we conducted an in-silico subtraction of nuclear and cytoplasmic fractions (ΔNC), as done previously (Anand et al., 2018; Kakrana et al., 2018; Lachke et al., 2012). This data analysis approach allowed us to prioritize differences between the nuclear and cytoplasmic fractions within each treatment and time point. Then, we conducted a two-way ANOVA with an FDR of 0.01 to determine transcripts that display significant changes in their ΔNC values in response to nitrate treatments. We identified 402 DLTs in response to nitrate in Arabidopsis roots (Figure 1c, Supporting Information S5: Data Set 3). To evaluate whether DLT levels in the fractions reflect mRNA levels measured in whole cells, we added nuclear and cytoplasmic normalized counts for each DLT. As shown in the heatmaps in Figure 1c, the levels obtained by the addition of the fractions are comparable to those obtained by independent sequencing in the whole cells (Figure 1c). These datasets showed a correlation of 0.99 (Figure 1d), indicating that the sum of DLT levels in the subcellular fractions represents DLT levels in the whole cells.

To understand the nitrate response dynamics across time-course experiments and subcellular localization, we performed a hierarchical cluster analysis of the 402 DLTs. We obtained 13 clusters including 387 DLTs, by setting a correlation coefficient value of ≥0.5 and requiring at least five genes in each cluster. (Figure 1c; Supporting Information S2: Figure 6). We summarized the 13 clusters in five types of localization patterns in response to nitrate treatments: Nuclear reduction (NR), showing decreased mRNA levels in the nucleus, containing 81 genes; Cytoplasmic reduction (CR), showing decreased mRNA levels in the cytoplasm, containing 125 genes; Nuclear accumulation (NA), showing increased mRNA levels in the nucleus, containing 76 genes; Cytoplasmic accumulation (CA), showing increased mRNA levels in the cytoplasm, containing 72 genes; and Delayed-cytoplasmic accumulation (D), showing increased mRNA levels in the nucleus 20 min after the nitrate treatment but increased mRNA levels in the cytoplasm at later times, containing 33 genes (Figure 2a, Supporting Information S5: Data Set 3). We selected two representative genes from each pattern and measured mRNA levels at 20 and 120 min after nitrate treatments by RT-qPCR using oligo(dT) (Supporting Information S2: Figure 7). We successfully confirmed the localization patterns for all genes. In a few instances, particularly among genes exhibiting reduced expression patterns, we noted some discrepancies in the RNA levels over time. Nevertheless, the disparities between nutrient conditions and sample fractions remain consistent with the patterns identified through RNA sequencing. Our cell-fractionation/RNA-seq strategy allowed us to identify transcripts with differential localization in the nucleus and cytoplasm in response to the nitrate treatment in Arabidopsis roots. Our results reveal nucleocytoplasmic localization could contribute to regulating gene expression in response to nitrate treatments in plants.

To gain insight into the biological processes that are represented among DLTs, we analysed overrepresented gene ontology (GO) and Kyoto Encyclopedia of Genes and Genome (KEGG) terms. DLTs code for genes involved in metabolic processes (such as cofactor, nitrogen compound, carbohydrate, glycerolipid, energy metabolism), localization (anion and amino acid transport), and response to stimulus (Figure 2b, Supporting Information S6: Data Set 4, Supporting Information S7: Data Set 5). These results demonstrate that mRNAs with relevant functions for the nitrate response are differentially distributed in the cellular fractions.

We also investigated the impact of transcript isoforms on nucleocytoplasmic distributions in response to nitrate treatment. We compared the profile of individual transcript isoforms for DLT and identified 632 transcript isoforms from the 402 DLTs (Supporting Information S2: Figure 8A). Interestingly, 89.8% of the isoforms exhibited concordant behaviour (positive and significant correlation, $p < 0.05$) with the mRNA levels calculated for the cognate DLT (Supporting Information S2: Figure 8B). Cases where transcript isoforms did not correlate with the corresponding DLT, were genes with low expression levels (Supporting Information S2: Figure 8C). These results indicate that differential compartmentalization of most transcripts isoforms showed similar behaviour to cognate genes in response to nitrate treatments.

2.3 | mRNA synthesis and decay determine the nucleocytoplasmic distribution of mRNAs in response to nitrate treatment

Steady-state mRNA levels in the cell are defined by the balance between mRNA synthesis and degradation (Bahar Halpern et al., 2015; Gutiérrez et al., 2002; Hansen et al., 2018). To assess whether DLTs may exhibit changes in mRNA synthesis during nitrate treatment, we used RNPII chromatin immunoprecipitation sequencing (ChIP-seq) data obtained from our group under the same experimental conditions (Alvarez et al., 2019) and analysed RNPII occupancy in the DLTs and nitrate-responsive genes after nitrate treatments (Figure 3a, Supporting Information S8: Data Set 6). We did not observe changes in RNPII occupancy of repressed transcripts among the nuclear, cytoplasmic, and total fractions. On the other hand, transcripts with nuclear, cytoplasmic, and delayed-cytoplasmic accumulation showed higher values of RNPII occupancy as compared with the total fraction. When we compared the RNPII recruitment for induced DLTs with genes with similar induction by nitrate in the total fraction, we observed significant differences in RNPII recruitment in induced DLTs compared with other induced genes. (Supporting Information S2: Figure 9A). In addition, we noticed that the majority

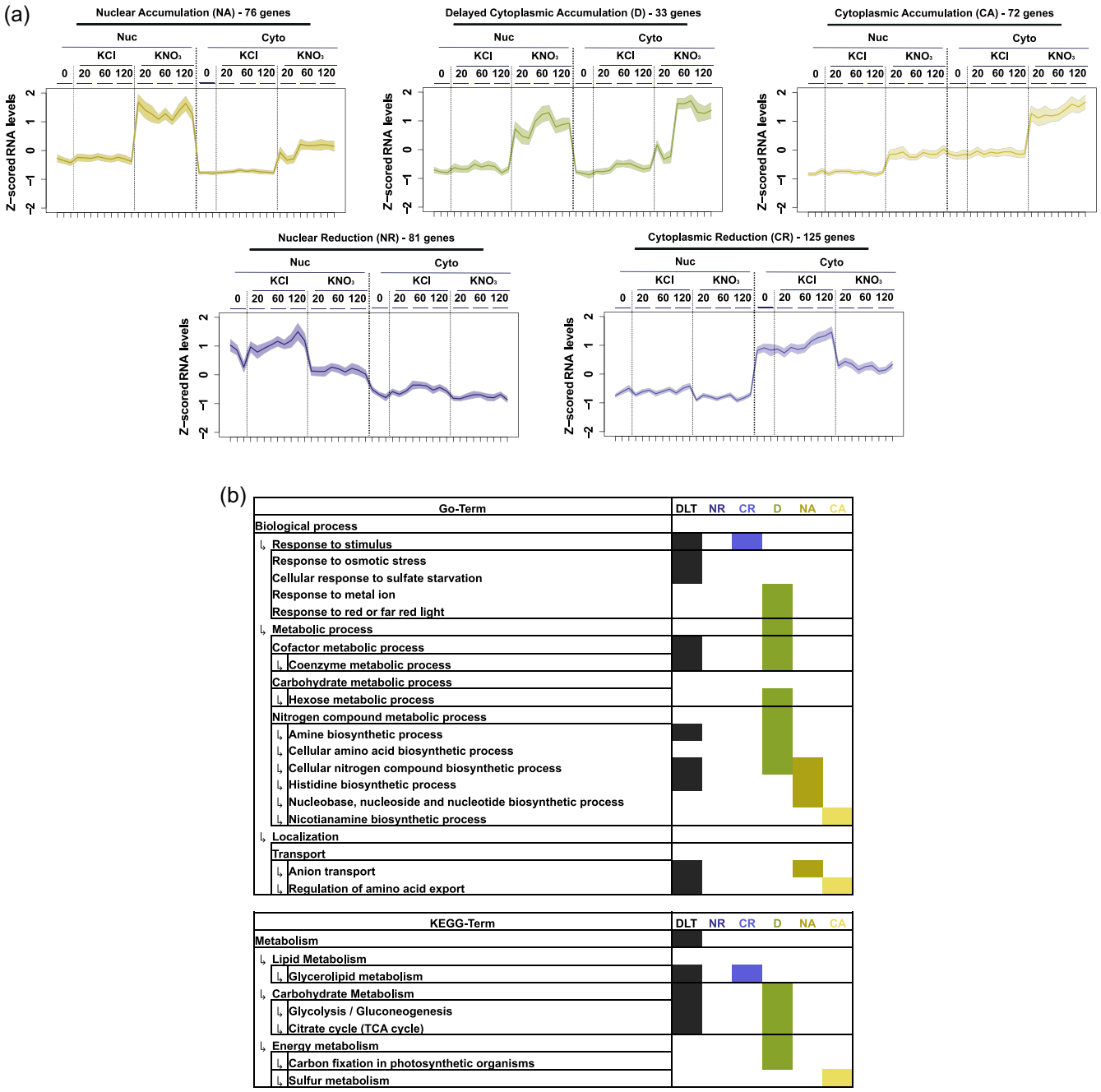

FIGURE 2 DLT localization patterns in response to nitrate treatments. (a) Five different localization patterns in response to nitrate treatments. DLTs were separated by the cellular fraction where the main changes were observed (Nuclear—Nuc—or cytoplasmic—Cyto) and if they showed an accumulation or reduction of mRNA levels in the nitrate condition. Graphs show mean values of *z*-scored normalized mRNA levels (line) and 95% confidence interval for mean values of each DLT for the three independent experiments (shadow). (b) Summary of significant ($p < 0.05$) overrepresentation of gene-ontology (GO, top), and KEGG-Terms (bottom) enriched in the lists of DLTs according to the VirtualPlant output (Katari et al., 2010). GO-terms were summarized by nonredundant 5 and 6 levels using REVIGO (Supek et al., 2011). CA, cytoplasmic accumulation; CR, cytoplasmic Reduction; D, delayed cytoplasmic accumulation; DLT, differentially localized transcript; NA, nuclear accumulation; NR, nuclear reduction. [Color figure can be viewed at wileyonlinelibrary.com]

of induced DLTs genes exhibited higher RNPII recruitment at 12 min as compared with 120 min, suggesting a robust and transient transcriptional activation or transcriptional burst (Supporting Information S2: Figure 9B). To determine the role of decay in the expression of DLTs after nitrate treatment, we performed RNA-seq of rRNA-depleted RNA from roots treated with KNO_3 or KCl for 120 min and then treated with cordycepin to measure RNA decay rates and estimate half-lives (Gutiérrez et al., 2002; Nagarajan et al., 2019). Normalized counts were used to model decay rates using an exponential adjustment for RNA levels as a function of time

(Gutiérrez et al., 2002; Narsai et al., 2007; Sorenson et al., 2018). We observed that most repressed mRNAs did not change half-lives in response to nitrate treatment. However, transcripts with delayed-cytoplasmic, nuclear, and cytoplasmic accumulation patterns showed significantly shorter half-lives as compared with other nitrate-responsive genes (Figure 3b, Supporting Information S2: Figure 10A, Supporting Information S9: Data Set 7). We observed that the induced DLT genes exhibited an enrichment of genes associated with RNA destabilization caused by nitrate. Among these, delayed-cytoplasmic accumulation displayed the highest decay rates in response to nitrate treatments (Supporting Information S2: Figure 10B). Our result indicates that transcripts from induced DLTs genes show faster turnover rates in response to nitrate treatment.

Analysis of RNPII occupancy and half-lives in nitrate-responsive genes revealed a significant negative correlation between RNPII occupancy at 12 min and RNA decay at 120 min (Pearson

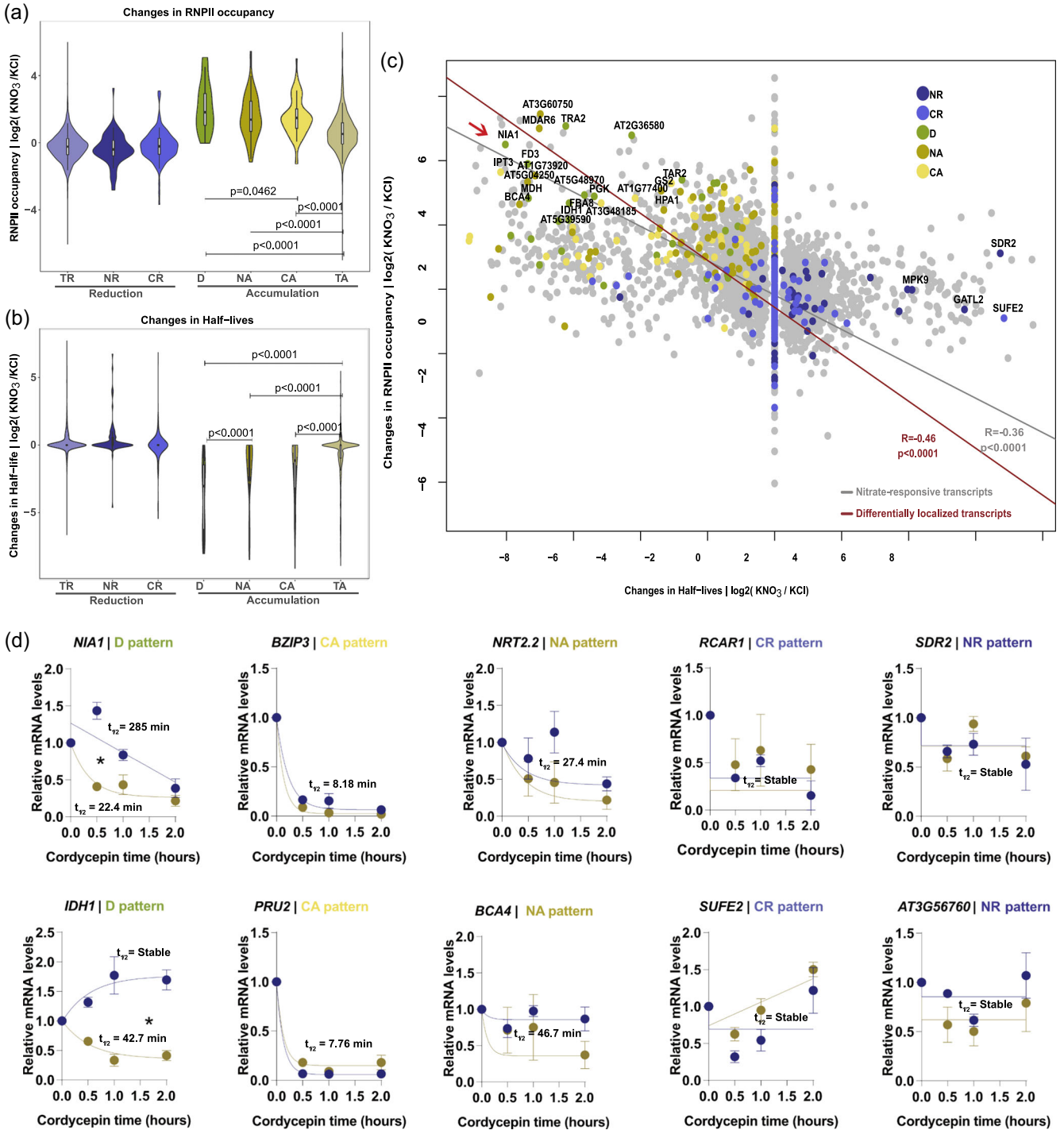

FIGURE 3 (See caption on next page).

correlation = −0.36, $p < 0.0001$) (Figure 3c). However, when comparing RNPII occupancy at 120 min with RNA decay, we observed a lower slope compared with RNPII occupancy at 12 min (Pearson correlation = −0.21, $p < 0.0001$) (Supporting Information S2: Figure 9C). Interestingly, when we only included DLTs in the comparison, we observed an even stronger negative correlation (Pearson correlation = −0.48, $p < 0.0001$). Among the top 5% in terms of mean rank for RNPII occupancy and half-life, we identified *NITRATE REDUCTASE 1* (*NIA1*) as the transcript with the largest differences (indicated by the red arrow in Figure 3d).

To further explore the relationship between nucleocytoplasmic mRNA distribution and stability, we chose representative genes from each localization pattern and measured mRNA levels at 20 and 120 min after nitrate treatments following cordycepin treatments (Figure 3d, Supporting Information S2: Figure 11). We observed that transcripts from the delayed-cytoplasmic accumulation pattern (*NIA1*, *IDH1*, *FBA8*, *CNX2*, *and FD3*) showed changes in their decay profile after different times of nitrate treatments. All transcripts are more stable after 20 min of treatments and decay faster after 120 min (Figure 3d, Supporting Information S2: Figure 11). On the contrary, all the other DLTs did not show significant changes in the decay profile between the evaluated times (Figure 3d). These results demonstrate that the control of mRNA localization, specifically in the D-pattern, could be a novel regulatory mechanism for modifying gene expression in response to nitrate treatments.

2.4 | Nucleocytoplasmic distribution of *NIA1* mRNA is associated with a strong transcriptional burst

NIA1 is involved in the first step of nitrate assimilation, specifically the conversion of nitrate to nitrite. The regulation of *NIA1* gene expression as well as the encoded protein activity is heavily influenced by various factors such as transcriptional control (Tang et al., 2022; Zhao et al., 2018), RNA degradation (Wu et al., 2020), and posttranslational modification (Costa-Broseta et al., 2021; Park et al., 2011; Tang et al., 2022). To gain a better understanding of how nitrate treatments affect the nucleocytoplasmic distribution of *NIA1*, we used single-molecule RNA FISH (smFISH) to visualize *NIA1* mRNA in single cells of Arabidopsis root squashes at 20 min (nuclear accumulation phase) and 120 min (cytoplasmic accumulation phase) after nitrate treatments (Figure 4a). The number of nuclear, cytoplasmic, and total mRNA molecules was counted using FISH-quant v3 (Mueller et al., 2013). The smFISH results for *NIA1* revealed big fluorescent foci located in the nucleus of nitrate-treated roots, indicating transcript accumulation of *NIA1* at active transcription sites (Figure 4b). As a contrast, no big nuclear foci were observed when the RNA of *PP2A*, a housekeeping gene, was detected in nitrate or control-treated roots (Supporting Information S2: Figure 12A). We observed a decrease in the number of nuclear fluorescence foci after cordycepin treatments (Supporting Information S2: Figure 12B) confirming those are coming from a large transcriptional activation in response to the nitrate treatment. Furthermore, there was an increase in the number of single molecule mRNAs of *NIA1* after 120 min of nitrate treatment, showing accumulation of *NIA1* mRNAs in the nucleoplasm and cytoplasm at later time (Figure 4b).

To quantify single molecules of *NIA1* in response to nitrate treatments, we calculated the number of transcripts considering single molecule counts and the estimated number of molecules in transcription sites. As expected, we observed more RNA molecules per cell area in the whole cell after nitrate treatment (Figure 4c). In addition, we found that the number of molecules increases in the cytoplasm more than within the nucleus 120 min after nitrate treatments (Figure 4d,e). This result is consistent with the delayed-cytoplasmic accumulation pattern described for *NIA1* transcripts in response to nitrate treatments. Moreover, we observed a greater number of RNAs at transcription sites (Figure 4g) and also greater number of active transcription sites per cell at 20 min after nitrate treatments (Figure 4h). However, we did not observe significant differences in nucleoplasm transcripts (Figure 4f) or in the intensity of transcription sites for the 20 min time-point (Figure 4i). This result indicates that nuclear accumulation of *NIA1*, 20 min after nitrate

FIGURE 3 Changes in RNA polymerase II (RNPII) occupancy and half-lives for DLTs in response to nitrate treatments. (a) Changes in RNPII occupancy after 12 min of treatments. (b) Changes in half-lives after 120 min of nitrate treatment. Violin plots show the distribution for DLTs in each pattern. We also include nitrate-regulated genes in the total fraction that are not differentially localized as a control (TA—Total accumulated, or TR—Total reduced). Boxes inside show the interquartile range (IQR - 25%–75%), indicating the median value as a horizontal line. Whiskers show the ±1.58 × IQR value. We compared the distributions using one-way ANOVA and Dunnett posttest. We include *p* values and brackets to highlight relevant comparisons. (c) Scatter plot showing the relationship between changes in RNPII occupancy and half-lives for all genes that respond to nitrate in any cellular fraction. Linear regression and Pearson correlation coefficient are indicated for all data (grey) and DLTs only (red). The red arrow shows *NIA1* as the DLT with the biggest changes in RNPII occupancy as well as half-life values. (d) Comparison of decay profiles and half-lives (t1/2) after 20 (blue) or 120 min (yellow) of KNO3 treatment. RNA levels were measured by RT-qPCR after 0, 0.5, 1, and 2 h of cordycepin treatment. The DLT pattern that each gene represents is indicated next to the gene's name. For each transcript, we evaluated first-order decay models with different or the same decay rate for both treatment times. The model with the lowest Akaike Information Criterion (AIC) score was chosen, and the half-life value was indicated on the graph. We marked 'Stable' when the half-life value could not be estimated because the model did not fit a decay curve. Asterisks (*) indicate the cases where the decay profile is different between the treatment times. Error bars show standard error for three independent experiments. CA, cytoplasmic accumulation; CR, cytoplasmic reduction; D, delayed-cytoplasmic accumulation; DLT, differentially localized transcript; NA, nuclear accumulation; NR, nuclear reduction. [Color figure can be viewed at wileyonlinelibrary.com]

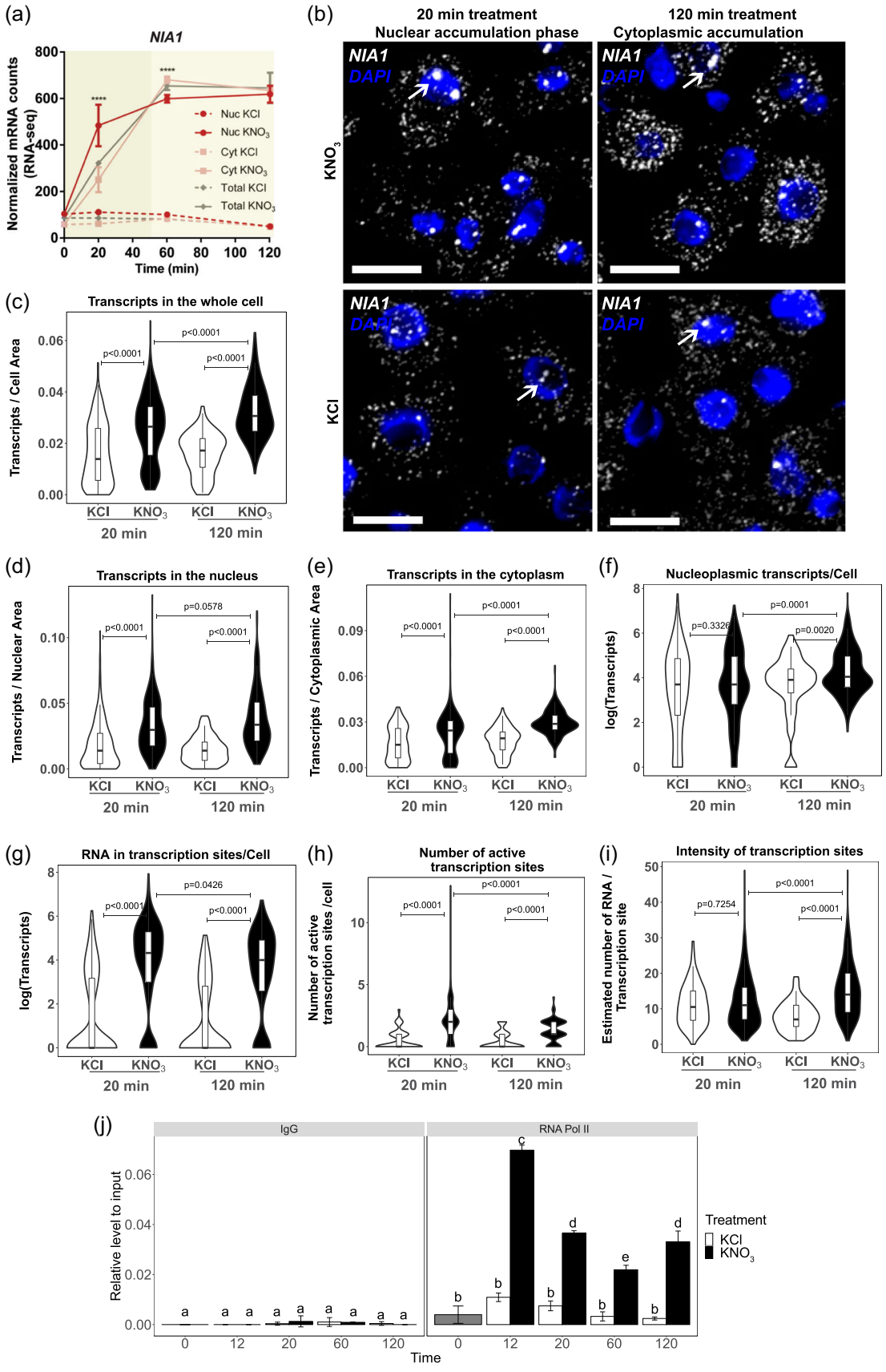

FIGURE 4 (See caption on next page).

treatments, derives from nascent RNAs or mRNAs accumulating at transcription sites. These results agree with a decrease in RNPII occupancy over time after nitrate treatments (Figure 4j).

3 | DISCUSSION

In this study, we described the nucleocytoplasmic dynamics of mRNA in response to nitrate treatments in *Arabidopsis thaliana* roots (Figure 5). We identified 1183 regulated genes in the subcellular fractions that are not detected as regulated when using whole cell RNA. Many of these genes were not identified as nitrate-regulated in previous studies despite extensive transcriptome analysis at the organism, organ and cell-type specific levels (Alvarez et al., 2019; Canales et al., 2014; Krouk et al., 2010; Swift et al., 2020; Varala et al., 2018; Wang et al., 2004). We described 402 DLTs in response to nitrate treatments using nuclear and cytoplasmic subcellular fractions coupled to transcriptome analysis. Specifically, induced DLTs exhibited significant changes in both synthesis and decay rates, suggesting rapid turnover of these mRNAs during the nitrate response. The identified DLTs include new N-responsive genes that code for relevant biological functions in the nitrate response. These findings highlight the relevance of modulating nucleocytoplasmic distribution for the control of gene expression in the plant's adaptive response to nitrogen nutrient signals.

In agreement with our results, a negative correlation between RNA synthesis and RNA half-lives has been reported for yeast, mouse, and fly cells under basal conditions (Chen & Van Steensel, 2017; Miller et al., 2011; Tippmann et al., 2012). Interestingly we found a stronger negative correlation when only DLTs were considered, comparable with the observed in *Saccharomyces cerevisiae*, where transcripts with specific functions in the osmotic stress response showed a stronger negative correlation (Miller et al., 2011). Increasing all RNA kinetic rates is a strategy for controlling transient induction and diminishing transcriptional noise (Rabani et al., 2014). For instance, rapid turnover occurs co-translationally in plants during the response to excess-light stress for faster tuning the genetic response to the stimulus (Crisp et al., 2017). This evidence suggests that DLTs undergo a faster replacement, probably due to their specific role in the cellular response to nitrate. Control of mRNA nucleocytoplasmic distribution would be another regulatory layer contributing to these transcripts' dynamic and transient expression.

Synthesis, export, and cytoplasmic decay rates are sufficient for mathematical modelling of the nucleocytoplasmic dynamics of mRNA (Bahar Halpern et al., 2015; Battich et al., 2015; Hansen et al., 2018), indicating that the mRNA nuclear degradation (Das et al., 2003) and extracellular export (Thieme et al., 2015) could not be considered in some cases. The synthesis and decay rates for DLTs transcripts do not explain all the differential distribution in the nucleus and cytoplasm in response to nitrate treatments. For example, transcripts with cytoplasmic accumulation showed a high RNPII occupancy and decay rate in response to nitrate treatments. Our results suggest nuclear export modulation could be an additional mechanism required to maintain low nuclear and high cytoplasmic levels (Figure 5). The mRNA nuclear export rates have been a strategy for controlling transient cellular responses under different cellular and environmental stimuli (Chen & Van Steensel, 2017; Lee & Bailey-Serres, 2019; Pastro et al., 2017). For example, nucleocytoplasmic dynamics of genes involved in response to stress showed a higher export rate than genes involved in constitutive functions in Drosophila and Arabidopsis (Chen & Van Steensel, 2017; Lee & Bailey-Serres, 2019). In this context, nitrate regulation of nuclear export might control several aspects of nucleocytoplasmic distribution of mRNA in response to nitrate treatments (Figure 5).

We observed different localization patterns for transcripts with distinct biological functions in response to nitrate treatments. We found mRNA cytoplasmic enrichment on genes coding for nitrogen-response transcriptional regulators (*BZIP3* and *VRN1*) (Figure 5) (Brooks et al., 2019), as well as genes involved in nutrient and amino acid homoeostasis (*NAS1/2* and *GDU1/2*) (Pratelli et al., 2010, 2012;

FIGURE 4 Dynamic changes in *NIA1* mRNA accumulation in transcription sites in response to nitrate treatments. (a) mRNA levels in cellular fractions measured by RNA-seq. (****) indicates statistical differences between nuclear and cytoplasmic fractions. (b) Representative microscope images from two independent experiments for *NIA1* RNA in situ detection in Arabidopsis root tip cells by RNA single molecule FISH (smFISH). White colour corresponds to fluorescent signal from Quasar570-associated probes for detecting exonic regions of *NIA1* mRNA. The blue colour corresponds to the DAPI stain. White arrows indicate examples of transcription sites for each image. Images are the result after a Dual-Gaussian filter using FISH-quant (Mueller et al., 2013). Scale bar = 10 µm. (c–i) Quantification of the RNA smFISH. Violin plots show the distribution for transcript quantification in the nitrate (KNO3, black) or control (KCl, white) conditions at 20 or 120 min after the treatment. Boxes inside show the interquartile range (IQR - 25%–75%), indicating the median value as a horizontal line. Whiskers show the ±1.58 × IQR value. Images from two independent experiments were analysed, including 6 roots/296 cells for KCl 20 min, 8 roots/334 cells for KNO3 20 min, 6 roots/293 cells for KCl 120 min, and 6 roots/257 cells for KNO3 120 min, (c) Estimated number of transcripts per cell area in whole cells (nucleus+cytoplasm). (d) Number of transcripts per nuclear area. The number of nucleoplasmic transcripts and the estimated number of molecules in transcription sites are included. (e) Number of cytoplasmic transcripts per area. (f) Number of transcripts in the nucleoplasm per cell in log2 scale. (g) Number of transcripts in transcription sites per cell in log2 scale. (h) Number of active transcription sites per cell. (i) Estimated number of transcripts in each transcription site (Number of transcription sites included: KCl 20 min—138, KNO3 20 min—319, KCl 120 min—69, KNO3 120 min—233) (j) RNPII-ChIP-qPCR to evaluate the RNPII occupancy at *NIA1* locus after 0, 12, 20, 60, and 120 min of KNO3 (black) or KCl (white) treatments. Bars show the mean ± standard deviation for three independent replicates. Quantification for unspecific IgG binding are included. Different letters show statistically significant differences ($p < 0.05$) for the two-way ANOVA/Tukey test (where treatment and time were used as factors). [Color figure can be viewed at wileyonlinelibrary.com]

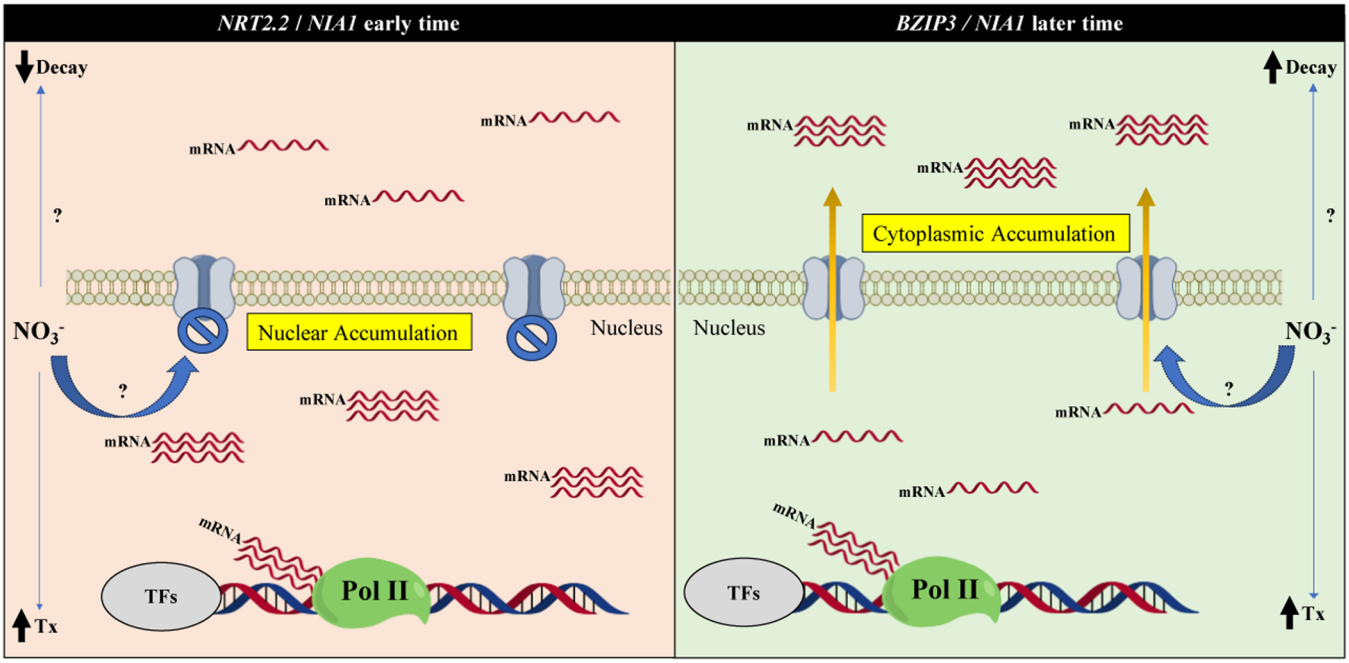

FIGURE 5 Model diagram for mRNA nucleocytoplasmic distribution in response to nitrate treatments. In response to nitrate (NO_3-), numerous mRNAs exhibit differential localization between the nucleus and cytoplasm. Upon nutrient perception, activation of various transcription factors leads to a strong and transient burst of transcription, resulting in the synthesis of mRNAs with critical biological functions. Some transcripts predominantly accumulate in the nucleus (e.g., those coding for the nitrate transporter NRT2.2), possibly due to limitations in nuclear export rates. These transcripts also exhibit longer half-lives and decreased decay rates. Conversely, certain transcripts, despite high synthesis rates, primarily accumulate in the cytoplasm (e.g., those coding for the transcription factor BZIP3). These transcripts have higher decay rates, suggesting the need for sustained cytoplasmic export. For the mRNA of nitrate reductase NIA1, early accumulation occurs in the nucleus, transitioning to cytoplasmic accumulation later. This dynamic pattern indicates temporal tuning of RNA kinetics. The mechanisms for the regulation of export and decay rates by nitrate remain an open question, nevertheless, the dynamic nucleocytoplasmic distribution evidence additional layers to the gene expression control in plant adaptation to nutritional signals. [Color figure can be viewed at wileyonlinelibrary.com]

Yu et al., 2015; Zhao et al., 2019). Similar mechanisms have been observed in HSP genes during the export from their transcripts into the cytoplasm of yeast in response to heat. (Saavedra et al., 1996; Zander et al., 2016). Considering that VRN1 and BZIP3 are TFs, we can expect that both regulators are preferentially exported to increase their expression, and in this way, efficiently control other genes involved in the nitrate response (Figure 5). In contrast, we also identified transcripts with nuclear accumulation that have a direct role in nitrogen metabolism and development, for instance, the transcripts for NRT2.2, SULTR1.1, HPA1 and HISN1A (Bao et al., 2011; De Pessemier et al., 2013; Kotur et al., 2012; Mo et al., 2006) (Figure 5). The differential accumulation of these transcripts can help prioritize mRNA translation of other transcripts, as nuclear-retained transcripts decrease their association with polysomes and protein synthesis (Benoit Bouvrette et al., 2018; Lee & Bailey-Serres, 2019; Pastro et al., 2017; Reynoso et al., 2019; Yeap et al., 2019). For example, the high-affinity nitrate transporter 2.2 (NRT2.2) plays an essential role in nitrate uptake (ref). In agricultural soils, nitrate shows strong spatial and temporal heterogeneity (ref). Therefore, the plant could accumulate *NRT2.2* transcripts in the nucleus to minimize energy requirements under conditions of limited reserves (Fredes et al., 2019). This kind of regulatory mechanism has been described in response to hypoxia in Arabidopsis (Lee et al., 2019) and suggested to be conserved in other angiosperms (Reynoso et al., 2019), highlighting the plants' ability to change transcripts' availability to adapt their physiological response to environmental stimuli.

The temporal retention of mRNAs in the nucleus has been defined as a strategy for controlling the expression of transcripts synthesized during bursts of transcription (Bahar Halpern et al., 2015; Tudek et al., 2019). Nuclear accumulation of transcripts has been related to the activation of RNA synthesis in Arabidopsis embryos (Palovaara & Weijers, 2019). The transcriptional burst requires temporal coupling between TFs and target motifs to activate a gene in response to a signal. The hit-and-run model posits that a TF can function as a trigger to assemble a stable transcriptional complex (including transcription machinery and, potentially, other TFs). Subsequently, transcription by RNA polymerase II can proceed without the TF being bound to the DNA (Schaffner, 1988). Interestingly, it has been reported that bZIP1 and NLP7, master TF on a genome-wide scale, control the expression of early nitrogen TFs and genes with biologically relevant functions through transcriptional bursts (Alvarez et al., 2020; Para et al., 2014). Thus, NLP7 or bZIP1 have an expansive effect on N responses genome wide with a small number of TF. The advantage of modulating nucleocytoplasmic distribution, coupled with a Hit-and-Run activation mechanism,

allows an organism to activate gene expression in response to a signal and control the distribution of synthesized transcripts to help prioritize mRNA translation.

The regulation of genes encoding nitrate signalling pathway has been extensively studied. *NIA1* encodes to the first step of nitrate assimilation (Cheng et al., 1988; Santos-Filho et al., 2014) and their regulation is strongly depending on transcriptional (Tang et al., 2022; Zhao et al., 2018), RNA degradation (Wu et al., 2020), and posttranslational modification (Costa-Broseta et al., 2021; Park et al., 2011; Tang et al., 2022). A recent study showed that *NIA1* RNA degradation generates many siRNAs, some of which regulate their own expression; this allows the plant to quickly adapt its metabolism in response to its nutritional state (Wu et al., 2020). In addition, we found that *NIA1* displayed a nuclear accumulation phase associated with transcriptional bursting at early time points, followed by a cytoplasmic accumulation phase at later time points, where it becomes less stable (Figure 5). The temporal control of *NIA1* nucleocytoplasmic RNA levels could be a strategy to control the plant metabolism according to the nutrient levels.

We described the mRNA nucleocytoplasmic dynamics in response to nitrate treatment in Arabidopsis roots. The patterns observed for DLTs can be partially explained by synthesis and decay rates. Control of nuclear-to-cytoplasmic export could be a mechanism to explain the delay in cytoplasmic mRNA accumulation (Figure 5). This strategy could prolong mRNA accumulation and play a role in coordinating the expression of multiple genes required for specific biological processes in response to nitrate treatments. Understanding how nitrate regulates gene expression in metabolism, growth, and development is essential for developing new biotechnological solutions in agriculture. Our research gives new insights into plants' posttranscriptional RNA regulation and provides insights into the role of mRNA nucleocytoplasmic localization in nitrogen nutrition.

4 | METHODS

4.1 | Plant growth and nitrate treatments

Arabidopsis thaliana seedlings (Col-0 ecotype) were grown in hydroponic media in the Phytatray system (Cat.P1552; Sigma) for 14 days, using ammonium succinate as the only nitrogen source [MS without NH_4NO_3 or KNO_3 (Cat. M407; PhytoTech Labs), supplemented with 0.5 mM ammonium succinate and 1 g/L sucrose, pH 5.7]. We treated the seedlings at the beginning of Day 15 (right after the lights turned on) with KNO_3 (or KCl as control) to a final concentration of 5 mM, according to Alvarez et al. (2014). Root tissue from three Phytatrays (~4500 seedlings) was collected at 0, 20, 60, and 120 min of treatment and immediately frozen in liquid nitrogen until processing. For experiment replicates, the treatments and tissue collection were repeated two to three times in independent experiments.

4.2 | Cell fractionation

Cell fractionation was achieved through differential centrifugation based on the protocol of Xu and Copeland (2012). Root tissue was ground in lysis buffer (20 mM Tris-HCl pH 7.4, 25% glycerol, 20 mM KCl, 2 mM EDTA, 2.5 mM MgCl2, 250 mM sucrose, 1 DTT mM, PMSF 1 mM, and heparin 0.5 mg/mL). Unfractionated tissue was stored from ground roots as a 'total' fraction. For fractionation, the material was consecutively filtered in 70 and 40 µm nylon filters, and centrifugated at 1500*g* for 10 min. The pellets obtained correspond to the nuclear fraction, and the supernatants collected correspond to the cytoplasmic fraction. For the nuclear fraction, the pellets were washed by adding Nuclei resuspension buffer with Triton (NRBT) (20 mM Tris-HCl pH 7.4, 25% glycerol, 2.5 mM KCl, 0.2% Triton X-100, 1 mM DTT, and 0.5 mg/mL heparin) and centrifuging again at 1500*g* for 10 min. The washing step was repeated twice with NRBT, and a final wash with NRB (same composition as NRBT but without Triton X-100) was done to remove the detergent. The nuclear pellets were resuspended in 0.5 mL of nuclear storage buffer (NSB) (20 mM Tris-HCl pH 7.4, 25% glycerol, 2.5 mM $MgCl_2$, 0.44 M sucrose, 1 mM DTT, heparin 0.5 mg/mL) and stored at −80°C until processing. For the cytoplasmic fractions, the supernatants of the first centrifugation step were transferred into a new tube, centrifuged (1500*g* for 10 min) and collected again. This process was repeated three times to remove remaining nuclei. Cytoplasmic collections were stored at −80°C until processing.

4.3 | Immunoblot analysis

Cellular fractions were used for immunoblot experiments to evaluate the purity of the fractionated material. Nuclear pellets were resuspended in Honda buffer (2.5% Ficoll 400, 5% Dextran T40, 0.4 M sucrose, 25 mM Tris-HCl pH 7.4, 10 mM $MgCl_2$, 10 mM β-mercaptoethanol, 0.5 mM PMSF, and cOmplete EDTA-free Protease Inhibitor Cocktail Tablet [Cat. 04693116001; Roche]) (Honda et al., 1966) for protein extraction. We took 20 µL of the total, nuclear, or cytoplasmic fractions and mixed them with a 2xSDS loading buffer (4% SDS, 0.2% bromophenol blue, 20% glycerol, 200 mM DTT). Samples were incubated at 95°C for 5 min and loaded in 15% polyacrylamide gels for SDS-PAGE. Proteins were transferred to polyvinylidene difluoride (PVDF) membrane (Cat. 2803; Fluoro-Trans® Carl Roth) using the Trans-Blot Turbo Transfer System (Bio-Rad) and blocked with 5% skimmed milk in 1X TBST buffer (20 mM Tris pH 7.6, 150 mM NaCl, Tween 20 0.1%). We cut the membrane into two pieces (around the marker for 40 kDa) to continue with the primary antibody incubation. The membrane piece containing the proteins with a molecular weight lower than 40 kDa was incubated for 1 h with polyclonal anti-H3 (Agrisera AS10 710, dilution 1:2500 in 5% skimmed milk TBST) to detect HISTONE 3 (nuclear marker). The piece containing the proteins with a molecular weight higher than 40 kDa was incubated for 1 h with polyclonal anti-Actin (Agrisera AS13 2640, dilution 1:2000 in 2% BSA TBST) to detect ACTIN1/2/3/

4/5/7/8/11/12 (cytoplasmic markers). A 1:3000 dilution of Goat Anti-Rabbit IgG (H+L)-HRP Conjugate (Cat. 1706515; BioRad) in TBST was used as a secondary antibody for both cases. Immunoreaction was developed using the Pierce® ECL Western Blotting Substrate (Cat. 2109; Thermo Fisher Scientific) and detected in a LAS-3000 Luminescent Image Analyzer (Fujifilm, Fuji Photo Film). Quantitative analyses of the immunoblot results were performed with ImageJ, normalizing the pixel intensity values of the band for a reference protein detected in a gel stained with Coomassie blue.

4.4 | RNA extraction

RNA extraction from all cellular fractions was performed using an acid phenol-chloroform protocol based on (Darnell, 2012). Grinded tissue (total fraction) and nuclear pellets were resuspended in lysis buffer (0.1 M Tris-HCl pH 8.0, 10 mM EDTA, 1% SDS, 40 U/µL RNasin® Ribonuclease Inhibitor [Cat. N2511; Promega]). An aliquot of 2 mL of cytoplasmic fraction separated for RNA extraction. Samples were treated with Proteinase K (Cat. MC5005; Promega) for 1 h at 65°C. One volume of acidic phenol:chloroform:isoamyl alcohol (125:24:1) solution was added and incubated for 5 min at 28°C while shaking. Samples were centrifuged at 13 000 rpm for 10 min and the aqueous phase was recovered. RNA was precipitated by adding one volume of ethanol, 1/10 volume of 3 M sodium acetate, glycogen (Cat. R0551; Thermo Fisher Scientific) to a final concentration of 0.05 µg/µL and incubated overnight at −20°C. Samples were centrifuged at 12 000 rpm at 4°C for 20 min and pellets were washed with 75% ethanol twice. RNA pellets were resuspended in nuclease-free water. All extracted RNA samples were purified following the Clean-up for Liquid Samples protocol from PureLink® RNA Mini Kit (Cat, 12183018A; Ambion). Concentration, integrity, and purity parameters were evaluated by capillary electrophoresis (Fragment Analyzer, STANDARD SENSITIVITY RNA ANALYSIS KIT DNF-471; Advanced Analytical Technologies) and spectrophotometry (Nanodrop2000; Thermo Scientific). We obtained at least 2 mg of RNA, RNA Quality Number (RQN) higher than 6.0, and optimal absorbance ratios (A260/A280 and A260/A230) for each extraction.

4.5 | RT-qPCR measurements

cDNA was synthesized from nuclear and cytoplasmic RNA using Improm II RT (Cat. #A3800; Promega), and cDNA levels were measured by qPCR using the Brilliant III Ultra-Fast qPCR Kit (Cat. #600880; Agilent Technologies) and the StepOnePlus™ qPCR System (Agilent Technologies). Primers listed in Supporting Information S1: Table 1 were used for qPCR measurements. cDNA levels were calculated using the LinRegPCR software (Ramakers et al., 2004).

We selected two representative transcripts from each localization pattern for RT-qPCR experiments. These candidates have high expression levels and interesting functions in the nitrate response. The evaluated genes are *MPK9*, *AT3G56760*, *SUFE2*, *RCAR1*, *NRT2.2*, *BCA4*, *BZIP3*, *PRU2*, *NIA1*, and *IDH1*. The mean RNA levels for *CLATHRIN COAT ASSEMBLY* and *PP2AA* were used as normalizer factors. For RNA decay evaluation by qPCR, the mean level of *RAN3* and *MON1* was used as a normalizer factor. For both experimental designs, the best pair of normalizer genes was chosen by following the strategy described by (Remans et al., 2014), using NormFinder (Andersen et al., 2004). cDNA was synthesized using the oligo(dT) 5'-TTTTTTTTTTTTTTTTTTTTV-3. The qPCR experiments include three measurements from three independent experiments.

4.6 | RNA sequencing from cellular fractions

cDNA libraries from PolyA enriched RNA for three independent experiments were prepared by Macrogen service. We used the TruSeq® Stranded mRNA LT Sample Preparation Kit (Cat. RS-122-2101; Illumina) for library synthesis from RNA from each cellular fraction (nuclear, cytoplasmic, and total) for control (KCl) and treated (KNO_3) conditions for the four time-points collected (0, 20, 60, and 120 min). Libraries were sequenced in the Illumina Novaseq. 6000 platform with 100 bp paired-end reads by Macrogen.

4.7 | RNA-seq data analysis

R software packages (CRAN R Project) and custom-made scripts were used for data analysis. The FastQC software (0.10.0 version; Babraham Bioinformatics) was used to check the reads' quality, and then sequences were processed with Trimmomatic v0.36 (Bolger et al., 2014) to remove low-quality reads. Sequences that passed the quality criteria were mapped to the *Arabidopsis thaliana* genome (Araport11 annotation) using HISAT2 (Kim et al., 2015). We counted the reads at the level of gene locus, and used Rsubread R Library (Liao et al., 2013) to calculate the number of reads in TPM. We normalized the counts by molecule length and sequencing efficiency (Abrams et al., 2019).

In parallel, to analyse the abundance of transcript isoforms, Illumina sequencing samples were mapped against Arabidopsis Araport11 cDNA, using Kallisto (Bray et al., 2016). The subsequent analysis was conducted using the 3D RNA-seq pipeline (Guo et al., 2021). Transcript abundance was imported using the lengthScaledTPM method from tximport (Soneson et al., 2016) in the 3D RNA-seq pipeline.

We used quantile normalization to identify differentially expressed genes in the cellular fractions (Smyth, 2005). This strategy allows for ranking the RNA levels within each fraction and diminishes possible bias generated by technical differences in the fractionation protocol (Hansen et al., 2012). Nuclear and cytoplasmic TPMs were quantile normalized together (for comparisons between cellular fractions), and total TPMs were

analysed separately. To identify genes that are differentially accumulated by the treatment and change during the time course, a two-way ANOVA model was performed from the quantile normalized counts (in log2 scale) of each cellular fraction, evaluating the effects of treatment (KCl and KNO_3), time (20, 60, 120 min) and their interaction through the model. In this way, transcripts that fit the model with a significant p-value for treatment (T) or its interaction with time (Treatment:Time) were considered as genes whose mRNA levels change within the cellular fraction in response to nitrate treatments.

To compare the fractions, we thought it was important to consider the nuclear and cytoplasmic levels as dependent factors. Significant changes in one compartment will alter the transcript accumulation in the other, considering that both fractions were obtained from the same tissue. To solve this problem, we used the ΔNC value (Normalized counts in nuclear fraction minus normalized counts in cytoplasmic fraction) to measure nucleocytoplasmic distributions. Previously, in silico subtraction-based normalization has been effective for identifying tissue-enriched genes (Anand et al., 2018; Kakrana et al., 2018; Lachke et al., 2012). This simple arithmetic correction allowed us to evaluate if the RNA localization changes in dependence on the treatments and time using a two-way ANOVA. The transcripts whose ΔNC values fit the ANOVA model with a significant *p* value (<0.01) for treatment or its interaction with time were considered DLTs in response to the nitrate treatments.

The different lists of regulated genes were compared using the Sungear software (Poultney et al., 2007). The Multiple Experiment Viewer (MeV) software (Saeed et al., 2003) was used to visualize and cluster the data. Gene groups were defined by hierarchical clustering from their Pearson correlation, using an average linkage method and defining a threshold distance of 0.5. Enrichment analysis of GO and KEGG terms was performed using the BioMaps software from VirtualPlant v1.3 (Katari et al., 2010), selecting terms with a *p* value with FDR correction lower than 0.05. GO terms were summarized with REVIGO (http://revigo.irb.hr) set to obtain a medium-size list of terms according to Resnik similarity (Supek et al., 2011).

To compare the lists of regulated genes with the previously reported in transcriptomic studies in response to nitrate, the differentially expressed protein-coding genes were extracted from the respective supplementary data for: Alvarez et al. (2019); Canales et al. (2014); Krouk et al. (2010); Liu et al. (2022); Swift et al. (2020); Xiao et al. (2022). Furthermore, we included the lists for regulated genes in root tissues for Wang et al., 2004, and Varala et al., 2018. Additionally, the raw data from Cheng et al. (2023) was downloaded from the NCBI GEO (Gene Expression Omni; http://www.ncbi.nlm.nih.gov/geo/) under accession number GSE229228. The data was re-analysed using the R package 'RankProd' (Hong et al., 2006), choosing those genes with an FDR lower than 0.05. The R package 'UpSetR' (Conway et al., 2017) was used to represent the intersection of the previous lists in an UpSet plot.

4.8 | RNA stability evaluation

Arabidopsis thaliana seedlings were treated with a transcription inhibitor after the treatment with the nutrient, and RNA decay rates and half-lives were calculated for each condition (KNO_3 and KCl). Fourteen-day-old *Arabidopsis thaliana* seedlings were treated as described above. After 20 or 120 min of nutrient treatment, the plants were transferred to a solution of cordycepin 0.6 mM (Cat. #C3394; Sigma) prepared in MS without nitrogen (Cat. #M407; PhytoTechnology Laboratory), supplemented with 0.5 mM ammonium succinate and 1 g/L sucrose, pH 5.7. The treatments were performed in regular growth condition with low agitation. Roots were collected at 0, 30, 60, and 120 min after the cordycepin treatment for three independent experiments. RNA was extracted using TRIzol™ reagent (Cat. 15596; Invitrogen) following the protocol described by Macrae (2007). RNA was used for cDNA synthesis and subsequent quantification by RNA-seq (for RNA from seedlings treated for 120 min with nitrate) or qPCR to evaluate stability at other treatment times.

For RNA-seq analysis, 24 different libraries were synthesized from RNA extracted from three experiments (separate plant material grown independently). cDNA libraries (from rRNA-depleted RNA) were prepared by Macrogen service with TruSeq® Stranded Total RNA Library Prep Plant (Cat. 20020611; Illumina) using RNA from nitrate or control conditions after cordycepin treatment. The rRNA-depletion strategy was selected for not only investigating deadenylation-dependent decay events but also to encompass instances of 5′→3′ exonuclease- and endonuclease-mediated degradation. Libraries were sequenced by Macrogen in Illumina Novaseq. 6000 platform with 100 bp paired-end reads, requesting 40 million reads per sample. Raw data were analysed as described above for RNA-seq from cellular fractions until obtaining TPM normalized counts. The Multiple Experiment Viewer (MeV) (Saeed et al., 2003) software was used to visualize and cluster the data. Gene clusters were defined by hierarchical clustering from their Pearson squared correlation, using a complete linkage method, defining a threshold distance of 0.5.

Decay rates (k_{decay}) and then half-lives ($t_{1/2}$) were calculated by adjusting the measured RNA levels (*C*) as an exponential function of time (t). The mathematical adjustment for *C*(*t*) was developed assuming a constant decay rate, according to the function: $C(t) = e^{-kdecay * t}$ (Gutiérrez et al., 2002; Narsai et al., 2007; Sorenson et al., 2018). 'RNA decay' R-package (Sorenson et al., 2018) was used for decay modelling for RNA-seq data. Models in which decay rate changed or not between KNO_3 and KCl treatments were evaluated, and the model with the lowest Akaike Information Criterion (AIC) statistics was selected. RT-qPCR validations for decay patterns were performed using the same protocol explained above but using random primers (Cat. C118A; Promega) for retro-transcription instead. Comparisons on the percentage of genes with changes in their RNA decay rates in response to nitrate treatments were performed using the Genesect software from VirtualPlant v1.3 (Katari et al., 2010).

4.9 | RNA polymerase II occupancy changes

Data from RNA Polymerase II Chromatin Immunoprecipitation sequencing (RNPII-ChIPseq) was analysed (Alvarez et al., 2019). This data was obtained from *Arabidopsis thaliana* roots treated for 12 min with nitrate in the same conditions used to identify DLTs from two independent experiments. Furthermore, new treatments were performed to analyse RNPII after 120 min of treatments. For these assays, the protocol from Saleh et al. (2008). was followed. Briefly, plants grown in hydroponics, as indicated above, were treated with 5 mM KNO3 or 5 mm KCl for 120 min. Immediately at the end of the treatment, the roots were collected and fixed in 1% formaldehyde for 14 min under vacuum. Tissue from two independent experiments was collected. After nuclei enrichment, the chromatin was sonicated with a Bioruptor sonicator (UCD-200; Diagenode) with the following settings: 25 cycles of 30 s on, 30 s off with 5 min rest between every five cycles. A proportion of the chromatin was removed to use it as the input control. Each ChIP for KNO_3 and KCl treatment was performed in one biological replicate. The commercial antibody against RNPII (Ab817; Abcam) was used. Resulting DNA from was pooled to either qPCR experiments or to generate the sequencing library using TruSeq DNA Sample Prep Kit (Illumina). ChIP and Input DNA were used to sequence single-read ChIP-seq as per the manufacturer's instructions for 100 bp with a depth of 23.40, 22.07, 24.00, and 27.68 million reads for RNPII KNO_3 120 min, RNPII KCl 120 min, input KNO_3 120 min, and input KCl 120 min, respectively.

Read mapping of ChIP-seq results was performed with Bowtie2 (10.1038/nmeth.1923). Only the reads mapped to a unique position of the *A. thaliana* genome were used for further analysis. To evaluate the occupancy levels of RNPII on the genes for Figure 4j, we calculate the normalized sequence counts in regions spanning 500 bp upstream of the TSS, gene body, and 500 bp downstream of the TTS of protein-coding genes.

4.10 | RNA single-molecule FISH

RNA single-molecule Fluorescence in situ Hybridization (RNA smFISH) was performed according to the protocol described in Duncan et al. (2017). Forty-eight probes were designed using the Stellaris Probe Designer software (version 2.0 from Biosearch Technologies) to recognize exonic regions for the *NIA1* transcript. Probes with Quasar670 fluorophores were synthesized by Stellaris. To detect *PP2A* mRNA, we used probes that recognize exonic regions of the molecule associated with Quasar570 fluorophores as reported by Rosa et al. (2016). Probe sequences for both transcripts are listed in Supporting Information S1: Table 2.

Fifteen-day-old *A. thaliana* seedlings were treated with nitrate (and KCl as control) for 20 and 120 min. Some of these plants were also treated with cordycepin 0.6 mM for 120 min after nutrient treatment for transcription site analysis (the same way as described above for the decay analysis). Roots were collected, fixed in 4% paraformaldehyde solution, and squashed on microscope slides to obtain cell monolayers. Tissues from two independent experiments were analysed. Fixed samples were hybridized with the probe set and then with DAPI 100 ng/mL. The visualization and imaging were performed with a Zeiss LSM800 inverted microscope, using an x63 water-immersion objective and a cooled quad-port CCD (charge-coupled device) ZEISS Axiocam 503 mono camera. The following wavelengths were used for fluorescence detection: for Quasar570, an excitation filter 533–558 nm was used, with signal detection at 570–640 nm; for Quasar670, an excitation filter 625–655 nm was used, with signal detection at 665–715 nm; for DAPI, an excitation filter of 335–383 nm with signal detection at 420–470 nm. A series of optical sections with z-steps of 0.22 µm were collected for all experiments. Maximum projections and analysis of three-dimensional pictures were performed using Fiji. Cell segmentation was performed from 2D-maximum projection images using Cellprofiler (Stirling et al., 2021), using the DAPI signal to seed the segmentation and then identifying the cell borders from the background signal in the Quasar670 channel through a watershed algorithm. For background subtraction and quantification, FISH-quant software was used (Mueller et al., 2013). Tutorial instructions for batch analysis for 'Mature mRNA quantification' and 'Nascent mRNA quantification' were followed (Mueller et al., 2013). To analyse single-cell mRNA counts, dots that passed the threshold for sigmaXY, pixel intensity, and amplitude parameters were normalized by nuclear, cytoplasmic, or total area. Areas were calculated from 2D-projection outlines. The cytoplasmic area and dots were estimated as the subtraction between cellular and nuclear values.

4.11 | Accession numbers

Accession numbers based on The Arabidopsis Information Resource (TAIR) (https://www.arabidopsis.org) for all genes examined in this study are: *NIA1* (AT1G77760), *RAN3* (AT5G55190), *CLATHRIN COAT ASSEMBLY PROTEIN* (AT4G24550), *PP2A* (AT1G13320), *MON1* (AT2G28390), *MPK9* (AT3G18040), *PROTEIN KINASE SUPERFAMILY PROTEIN* (AT3G56760), *SUFE2* (AT1G67810), *RCAR1* (AT1G01360), *NRT2.2* (AT1G08100), *BCA4* (AT1G70410), *BZIP3* (AT5G15830), *PRU2* (AT1G49230), *IDH1* (AT4G35260), *CNX2* (AT2G31955), *FBA8* (AT3G52930), *FD3* (AT2G27510). Sequence data from this article can be found in the National Center for Biotechnology Information Gene Expression Omnibus under the project accessions: PRJNA720236 (data from cellular fractions), PRJNA791353 (data from stability assays), and PRJNA887810 (for RNPII-ChIP-seq data).

ACKNOWLEDGEMENTS

We thank Luis Villarroel, Ph.D. (Pontificia Universidad Católica de Chile) for help with data normalization and statistics strategy; and Adrian Dauphinee, Ph.D. (Swedish University of Agricultural Sciences), for contributing with an aliquot for the anti-Actin antibody. This work was supported by grants from the Agencia Nacional de Investigación y Desarrollo (ANID), through (i) ANID–Millennium

Science Initiative Program-Millennium Institute for Integrative Biology (iBio) ICN17_022, (ii) Center for Genome Regulation (ICN2021_044), and (iii) FONDECYT 1180759 to Rodrigo A. Gutiérrez and 11230913 to Eleodoro Riveras; (iv) FONDECYT Postdoc 3220801 to Tomás C. Moyano, (v) FONDECYT 1210389 and Millennium Institute for Integrative Biology Grant ICN17_022 to José M. Alvarez; and (vi) CONICYT Beca Doctorado Nacional 21161516 to Alejandro Fonseca. This work was also supported by Vetenskapsrådet (2018-04101) and Knut och Alice Wallenbergs Stiftelse (2019-0206) to Stefanie Rosa, and NSF Plant Genome Grant NSF-PGRP: IOS-1840761 to José M. Alvarez.

CONFLICT OF INTEREST STATEMENT

The authors declare no conflict of interest.

DATA AVAILABILITY STATEMENT

The author responsible for the distribution of materials integral to the findings presented in this article in accordance with the policy described in the Instructions for Authors is: Rodrigo A. Gutiérrez (rgutierrez@bio.puc.cl). The data that support the findings of this study are openly available in Gene Expression Omnibus at https://www.ncbi.nlm.nih.gov/geo/, reference number PRJNA720236 | PRJNA791353 | SUB12111862.

ORCID

Eleodoro Riveras http://orcid.org/0000-0001-8924-3954

REFERENCES

Abdelmoez, M.N., Iida, K., Oguchi, Y., Nishikii, H., Yokokawa, R., Kotera, H. et al. (2018) SINC-seq: correlation of transient gene expressions between nucleus and cytoplasm reflects single-cell physiology. *Genome Biology*, 19, 66.

Abrams, Z.B., Johnson, T.S., Huang, K., Payne, P.R.O. & Coombes, K. (2019) A protocol to evaluate RNA sequencing normalization methods. *BMC Bioinformatics*, 20, 679.

Alboresi, A., Gestin, C., Leydecker, M., Bedu, M., Meyer, C. & Truong, H. (2005) Nitrate, a signal relieving seed dormancy in Arabidopsis. *Plant, Cell & Environment*, 28, 500–512.

Alvarez, J.M., Brooks, M.D., Swift, J. & Coruzzi, G.M. (2021) Time-based systems biology approaches to capture and model dynamic gene regulatory networks. *Annual Review of Plant Biology*, 72, 105–131.

Alvarez, J.M., Moyano, T.C., Zhang, T., Gras, D.E., Herrera, F.J., Araus, V. et al. (2019) Local changes in chromatin accessibility and transcriptional networks underlying the nitrate response in Arabidopsis roots. *Molecular Plant*, 12, 1545–1560.

Alvarez, J.M., Riveras, E., Vidal, E.A., Gras, D.E., Contreras-López, O., Tamayo, K.P. et al. (2014) Systems approach identifies TGA1 and TGA4 transcription factors as important regulatory components of the nitrate response of *Arabidopsis thaliana* roots. *The Plant Journal*, 80, 1–13.

Alvarez, J.M., Schinke, A.L., Brooks, M.D., Pasquino, A., Leonelli, L., Varala, K. et al. (2020) Transient genome-wide interactions of the master transcription factor NLP7 initiate a rapid nitrogen-response cascade. *Nature Communications*, 11, 1157.

Anand, D., Kakrana, A., Siddam, A.D., Huang, H., Saadi, I. & Lachke, S.A. (2018) RNA sequencing-based transcriptomic profiles of embryonic lens development for cataract gene discovery. *Human Genetics*, 137, 941–954.

Andersen, C.L., Jensen, J.L. & Ørntoft, T.F. (2004) Normalization of real-time quantitative reverse transcription-PCR data: a model-based variance estimation approach to identify genes suited for normalization, applied to bladder and colon cancer data sets. *Cancer Research*, 64, 5245–5250.

Andrews, M., Raven, J.A. & Lea, P.J. (2013) Do plants need nitrate? The mechanisms by which nitrogen form affects plants. *Annals of Applied Biology*, 163, 174–199.

Araus, V., Swift, J., Alvarez, J.M., Henry, A. & Coruzzi, G.M. (2020) A balancing act: how plants integrate nitrogen and water signals. *Journal of Experimental Botany*, 71, 4442–4451.

Bahar Halpern, K., Caspi, I., Lemze, D., Levy, M., Landen, S., Elinav, E. et al. (2015) Nuclear retention of mRNA in mammalian tissues. *Cell Reports*, 13, 2653–2662.

Bao, S., An, L., Su, S., Zhou, Z. & Gan, Y. (2011) Expression patterns of nitrate, phosphate, and sulfate transporters in Arabidopsis roots exposed to different nutritional regimes. *Botany*, 89, 647–653.

Barthelson, R.A., Lambert, G.M., Vanier, C., Lynch, R.M. & Galbraith, D.W. (2007) Comparison of the contributions of the nuclear and cytoplasmic compartments to global gene expression in human cells. *BMC Genomics*, 8, 340.

Battich, N., Stoeger, T. & Pelkmans, L. (2015) Control of transcript variability in single mammalian cells. *Cell*, 163, 1596–1610.

Benoit Bouvrette, L.P., Cody, N., Bergalet, J., Lefebvre, F.A., Diot, C., Wang, X. et al. (2018) CeFra-seq reveals broad asymmetric mRNA and noncoding RNA distribution profiles in Drosophila and human cells. *RNA*, 24, 98–113.

Bolger, A.M., Lohse, M. & Usadel, B. (2014) Trimmomatic: a flexible trimmer for Illumina sequence data. *Bioinformatics*, 30, 2114–2120.

Bray, N.L., Pimentel, H., Melsted, P. & Pachter, L. (2016) Near-optimal probabilistic RNA-seq quantification. *Nature Biotechnology*, 34, 525–527.

Brooks, M.D., Cirrone, J., Pasquino, A.V., Alvarez, J.M., Swift, J., Mittal, S. et al. (2019) Network Walking charts transcriptional dynamics of nitrogen signaling by integrating validated and predicted genome-wide interactions. *Nature Communications*, 10, 1569.

Canales, J., Contreras-López, O., Álvarez, J.M. & Gutiérrez, R.A. (2017) Nitrate induction of root hair density is mediated by TGA1/TGA4 and CPC transcription factors in *Arabidopsis thaliana*. *The Plant Journal*, 92, 305–316.

Canales, J., Moyano, T.C., Villarroel, E. & Gutiérrez, R.A. (2014) Systems analysis of transcriptome data provides new hypotheses about Arabidopsis root response to nitrate treatments. *Frontiers in Plant Science*, 5, 76238.

Castro Marín, I., Loef, I., Bartetzko, L., Searle, I., Coupland, G., Stitt, M. et al. (2011) Nitrate regulates floral induction in Arabidopsis, acting independently of light, gibberellin and autonomous pathways. *Planta*, 233, 539–552.

Chen, J., Sui, X., Ma, B., Li, Y. & Qiao, L. (2022) Arabidopsis CPR5 plays a role in regulating nucleocytoplasmic transport of mRNAs in ethylene signaling pathway. *Plant Cell Reports*, 41(4), 1075–1085. https://doi.org/10.1007/s00299-022-02838-1

Chen, T. & Van Steensel, B. (2017) Comprehensive analysis of nucleocytoplasmic dynamics of mRNA in Drosophila cells. *PLoS Genetics*, 13, e1006929.

Cheng, C.L., Dewdney, J., Nam, H.G., Den Boer, B.G. & Goodman, H.M. (1988) A new locus (NIA1) in *Arabidopsis thaliana* encoding nitrate reductase. *The EMBO Journal*, 7, 3309–3314.

Cheng, Y.H., Durand, M., Brehaut, V., Hsu, F.C. & Texier, Y. (2023) Interplay between NIN-LIKE PROTEINs 6 and 7 in nitrate signaling plant physiology. *Plant Physiology*, 192(4), 3049–3068. https://doi.org/10.1093/plphys/kiad242

Choudury, S.G., Shahid, S., Cuerda-Gil, D., Panda, K., Cullen, A., Ashraf, Q. et al. (2019) The RNA export factor ALY1 enables genome-wide RNA-directed DNA methylation. *The Plant Cell*, 31, 759–774.

Conway, J.R., Lex, A. & Gehlenborg, N. (2017) UpSetR: an R package for the visualization of intersecting sets and their properties. *Bioinformatics*, 33(18), 2938–2940. Available from: https://doi.org/10.1093/bioinformatics/btx364

Costa-Broseta, Á., Castillo, M. & León, J. (2021) Post-translational modifications of nitrate reductases autoregulates nitric oxide biosynthesis in arabidopsis. *International Journal of Molecular Sciences*, 22, 549.

Crisp, P.A., Ganguly, D.R., Smith, A.B., Murray, K.D., Estavillo, G.M., Searle, I. et al. (2017) Rapid recovery gene downregulation during excess-light stress and recovery in Arabidopsis. *The Plant Cell*, 29, 1836–1863.

Darnell, R. (2012) Identification of RNAs bound by a specific protein CLIP (Cross-Linking and Immunoprecipitation). *Cold Spring Harbor Protocols*, 2012, 1146–1160.

Dalmadi, A., Gyula, P., Bálint, J., Szittya, G. & Havelda, Z. (2019) AGO-unbound cytosolic pool of mature miRNAs in plant cells reveals a novel regulatory step at AGO1 loading. *Nucleic Acids Research*, 47(18), 9803–9817. Available from: https://doi.org/10.1093/nar/gkz690

Das, B., Butler, J.S. & Sherman, F. (2003) Degradation of normal mRNA in the Nucleus of *Saccharomyces cerevisiae*. *Molecular and Cellular Biology*, 23, 5502–5515.

Djebali, S., Davis, C.A., Merkel, A., Dobin, A., Lassmann, T., Mortazavi, A. et al. (2012) Landscape of transcription in human cells. *Nature*, 489, 101–108.

Duncan, S., Olsson, T., Hartley, M., Dean, C. & Rosa, S. (2017) Single molecule RNA FISH in Arabidopsis root cells. *Bio-Protocol*, 7, 1–10.

Ehrnsberger, H.F., Grasser, M. & Grasser, K.D. (2019) Nucleocytosolic mRNA transport in plants: export factors and their influence on growth and development. *Journal of Experimental Botany*, 70, 3757–3763.

Eser, P., Demel, C., Maier, K.C., Schwalb, B., Pirkl, N., Martin, D.E. et al. (2014) Periodic mRNA synthesis and degradation co-operate during cell cycle gene expression. *Molecular Systems Biology*, 10, 1–15.

Forde, B.G. & Walch-Liu, P. (2009) Nitrate and glutamate as environmental cues for behavioural responses in plant roots. *Plant, Cell & Environment*, 32, 682–693.

Fredes, I., Moreno, S., Díaz, F.P. & Gutiérrez, R.A. (2019) Nitrate signaling and the control of Arabidopsis growth and development. *Current Opinion in Plant Biology*, 47, 112–118.

Gaudinier, A., Rodriguez-Medina, J., Zhang, L., Olson, A., Liseron-Monfils, C., Bågman, A.M. et al. (2018) Transcriptional regulation of nitrogen-associated metabolism and growth. *Nature*, 563, 259–264.

Gifford, M.L., Dean, A., Gutierrez, R.A., Coruzzi, G.M. & Birnbaum, K.D. (2008) Cell-specific nitrogen responses mediate developmental plasticity. *Proceedings of the National Academy of Sciences*, 105, 803–808.

Gras, D.E., Vidal, E.A., Undurraga, S.F., Riveras, E., Moreno, S., Dominguez-Figueroa, J. et al. (2018) SMZ/SNZ and gibberellin signaling are required for nitrate- elicited delay of flowering time in *Arabidopsis thaliana*. *Journal of Experimental Botany*, 69, 619–631.

Gruber, B.D., Giehl, R.F.H., Friedel, S. & von Wirén, N. (2013) Plasticity of the Arabidopsis root system under nutrient deficiencies. *Plant Physiology*, 163, 161–179.

Guo, W., Tzioutziou, N.A., Stephen, G., Milne, I., Calixto, C., Waugh, R. et al. (2021) 3D RNA-seq: a powerful and flexible tool for rapid and accurate differential expression and alternative splicing analysis of RNA-seq data for biologists. *RNA Biology*, 18, 1574–1587.

Gutiérrez, R.A. (2012) Systems biology for enhanced plant nitrogen nutrition. *Science*, 336, 1673–1675.

Gutiérrez, R.A., Ewing, R.M., Cherry, J.M. & Green, P.J. (2002) Identification of unstable transcripts in Arabidopsis by cDNA microarray analysis: rapid decay is associated with a group of touch- and specific clock-controlled genes. *Proceedings of the National Academy of Sciences*, 99, 11513–11518.

Gutiérrez, R.A., Lejay, L.V., Dean, A., Chiaromonte, F., Shasha, D.E. & Coruzzi, G.M. (2007) Qualitative network models and genome-wide expression data define carbon/nitrogen-responsive molecular machines in Arabidopsis. *Genome Biology*, 8, R7.

Hansen, K.D., Irizarry, R.A. & Wu, Z. (2012) Removing technical variability in RNA-seq data using conditional quantile normalization. *Biostatistics*, 13, 204–216.

Hansen, M.M.K., Desai, R.V., Simpson, M.L. & Weinberger, L.S. (2018) Cytoplasmic amplification of transcriptional noise generates substantial cell-to-cell variability. *Cell Systems*, 7, 384–397.

Ho, C.H., Lin, S.H., Hu, H.C. & Tsay, Y.F. (2009) CHL1 functions as a nitrate sensor in plants. *Cell*, 138, 1184–1194.

Honda, S.I., Hongladarom, T. & Laties, G.G. (1966) A new isolation medium for plant organelles. *Journal of Experimental Botany*, 17, 460–472.

Hong, F., Breitling, R., McEntee, C.W., Wittner, B.S. & Nemhauser, J.L. (2006) RankProd: a bioconductor package for detecting differentially expressed genes in meta-analysis. *Bioinformatics*, 22(22), 2825–2827. Available from: https://doi.org/10.1093/bioinformatics/btl476

Hu, H.C., Wang, Y.Y. & Tsay, Y.F. (2009) AtCIPK8, a CBL-interacting protein kinase, regulates the low-affinity phase of the primary nitrate response. *The Plant Journal*, 57, 264–278.

Jovanovic, M., Rooney, M.S., Mertins, P., Przybylski, D., Chevrier, N., Satija, R. et al. (2015) Dynamic profiling of the protein life cycle in response to pathogens. *Science*, 347, 1–16.

Kakrana, A., Yang, A., Anand, D., Djordjevic, D., Ramachandruni, D., Singh, A. et al. (2018) ISyTE 2.0: a database for expression-based gene discovery in the eye. *Nucleic Acids Research*, 46, D875–D885.

Katari, M.S., Nowicki, S.D., Aceituno, F.F., Nero, D., Kelfer, J., Thompson, L.P. et al. (2010) VirtualPlant: a software platform to support systems biology research. *Plant Physiology*, 152, 500–515.

Kim, D., Langmead, B. & Salzberg, S.L. (2015) HISAT: a fast spliced aligner with low memory requirements. *Nature Methods*, 12, 357–360.

Kim, J.-E., Hong, Y.H., Kim, J.Y., Jeon, G.S., Jung, J.H., Yoon, B.N. et al. (2017) Altered nucleocytoplasmic proteome and transcriptome distributions in an in vitro model of amyotrophic lateral sclerosis. *PLoS One*, 12, e0176462.

Kotur, Z., Mackenzie, N., Ramesh, S., Tyerman, S.D., Kaiser, B.N. & Glass, A. (2012) Nitrate transport capacity of the *Arabidopsis thaliana* NRT2 family members and their interactions with AtNAR2.1. *New Phytologist*, 194, 724–731.

Krouk, G., Mirowski, P., Lecun, Y., Shasha, D.E. & Coruzzi, G.M. (2010) Predictive network modeling of the high-resolution dynamic plant transcriptome in response to nitrate. *Genome Biology*, 11, R123.

Krouk, G., Tranchina, D., Lejay, L., Cruikshank, A.A., Shasha, D., Coruzzi, G.M. et al. (2009) A systems approach uncovers restrictions for signal interactions regulating genome-wide responses to nutritional cues in Arabidopsis. *PLoS Computational Biology*, 5, e1000326.

Lachke, S.A., Ho, J., Kryukov, G.V., O'Connell, D.J., Aboukhalil, A., Bulyk, M.L. et al. (2012) iSyTE: integrated systems tool for eye gene discovery. *Investigative Opthalmology & Visual Science*, 53, 1617–1627.

Landrein, B., Formosa-Jordan, P., Malivert, A., Schuster, C., Melnyk, C.W., Yang, W. et al. (2018) Nitrate modulates stem cell dynamics in Arabidopsis shoot meristems through cytokinins. *Proceedings of the National Academy of Sciences*, 115, 1382–1387.

Lee, T.A. & Bailey-Serres, J. (2019) Integrative analysis from the epigenome to translatome uncovers patterns of dominant nuclear regulation during transient stress. *The Plant Cell*, 31, 2573–2595.

de Leone, M.J., Hernando, C.E., Romanowski, A., Careno, D.A., Soverna, A.F., Sun, H. et al. (2020) Bacterial infection disrupts clock gene expression to attenuate immune responses. *Current Biology*, 30, 1740–1747.

Liao, Y., Smyth, G.K. & Shi, W. (2013) The Subread aligner: fast, accurate and scalable read mapping by seed-and-vote. *Nucleic Acids Research*, 41, e108.

Liu, K.H., Liu, M., Lin, Z., Wang, Z.F., Chen, B., Liu, C. et al. (2022) NIN-like protein 7 transcription factor is a plant nitrate sensor. *Science*, 377, 1419–1425.

Liu, K.H. & Tsay, Y.F. (2003) Switching between the two action modes of the dual-affinity nitrate transporter CHL1 by phosphorylation. *The EMBO Journal*, 22, 1005–1013.

Macrae, E. (2007) Extraction of plant RNA. *Methods in Molecular Biology*, 353, 15–24.

Martin, W. & Koonin, E.V. (2006) Introns and the origin of nucleus–cytosol compartmentalization. *Nature*, 440, 41–45.

Miller, C., Schwalb, B., Maier, K., Schulz, D., Dümcke, S., Zacher, B. et al. (2011) Dynamic transcriptome analysis measures rates of mRNA synthesis and decay in yeast. *Molecular Systems Biology*, 7, 1–13.

Mo, X., Zhu, Q., Li, X., Li, J., Zeng, Q., Rong, H. et al. (2006) The hpa1 mutant of Arabidopsis reveals a crucial role of histidine homeostasis in root meristem maintenance. *Plant Physiology*, 141, 1425–1435.

Moreno, S., Canales, J., Hong, L., Robinson, D., Roeder, A. & Gutiérrez, R.A. (2020) Nitrate defines shoot size through compensatory roles for endoreplication and cell division in Arabidopsis thaliana. *Current Biology*, 30, 1988–2000.

Mueller, F., Senecal, A., Tantale, K., Marie-Nelly, H., Ly, N., Collin, O. et al. (2013) FISH-quant: automatic counting of transcripts in 3D FISH images. *Nature Methods*, 10, 277–278.

Nagarajan, V.K., Kukulich, P.M., Von Hagel, B. & Green, P.J. (2019) RNA degradomes reveal substrates and importance for dark and nitrogen stress responses of Arabidopsis XRN4. *Nucleic Acids Research*, 47, 9216–9230.

Narsai, R., Howell, K.A., Millar, A.H., O'Toole, N., Small, I. & Whelan, J. (2007) Genome-wide analysis of mRNA decay rates and their determinants in *Arabidopsis thaliana*. *The Plant Cell*, 19, 3418–3436.

O'Brien, J.A., Vega, A., Bouguyon, E., Krouk, G., Gojon, A. & Coruzzi, G. et al. (2016) Nitrate transport, sensing and responses in plants. *Molecular Plant*, 837, 856.

Owen, A.G. & Jones, D.L. (2001) Competition for amino acids between wheat roots and rhizosphere microorganisms and the role of amino acids in plant N acquisition. *Soil Biology and Biochemistry*, 33, 651–657.

Palovaara, J. & Weijers, D. (2019) Adapting INTACT to analyse cell-type-specific transcriptomes and nucleocytoplasmic mRNA dynamics in the Arabidopsis embryo. *Plant Reproduction*, 32, 113–121.

Para, A., Li, Y., Marshall-Colón, A., Varala, K., Francoeur, N.J., Moran, T.M. et al. (2014) Hit-and-run transcriptional control by bZIP1 mediates rapid nutrient signaling in Arabidopsis. *Proceedings of the National Academy of Sciences*, 111, 10371–10376.

Park, B.S., Song, J.T. & Seo, H.S. (2011) Arabidopsis nitrate reductase activity is stimulated by the E3 SUMO ligase AtSIZ1. *Nature Communications*, 2, 400.

Parry, G. (2015) The plant nuclear envelope and regulation of gene expression. *Journal of Experimental Botany*, 66, 1673–1685.

Pastro, L., Smircich, P., Di Paolo, A., Becco, L., Duhagon, M.A., Sotelo-Silveira, J. et al. (2017) Nuclear compartmentalization contributes to stage-specific gene expression control in Trypanosoma cruzi. *Frontiers in Cell and Developmental Biology*, 5, 1–14.

Patterson, K., Cakmak, T., Cooper, A., Lager, I.D.A., Rasmusson, A.G. & Escobar, M.A. (2010) Distinct signalling pathways and transcriptome response signatures differentiate ammonium- and nitrate-supplied plants. *Plant, Cell and Environment*, 33, 1486–1501.

De Pessemier, J., Chardon, F., Juraniec, M., Delaplace, P. & Hermans, C. (2013) Natural variation of the root morphological response to nitrate supply in *Arabidopsis thaliana*. *Mechanisms of Development*, 130, 45–53.

Pfaff, C., Ehrnsberger, H.F., Flores-Tornero, M., Sørensen, B.B., Schubert, T., Längst, G. et al. (2018) ALY RNA-binding proteins are required for nucleocytosolic mRNA transport and modulate plant growth and development. *Plant Physiology*, 177, 226–240.

Poitout, A., Crabos, A., Petřík, I., Novák, O., Krouk, G., Lacombe, B. et al. (2018) Responses to systemic nitrogen signaling in Arabidopsis roots involve trans-zeatin in shoots. *The Plant Cell*, 30, 1243–1257.

Poultney, C.S., Gutiérrez, R.A., Katari, M.S., Gifford, M.L., Paley, W.B., Coruzzi, G.M. et al. (2007) Sungear: interactive visualization and functional analysis of genomic datasets. *Bioinformatics*, 23, 259–261.

Pratelli, R., Guerra, D.D., Yu, S., Wogulis, M., Kraft, E., Frommer, W.B. et al. (2012) The ubiquitin E3 ligase LOSS OF GDU2 is required for GLUTAMINE DUMPER1-induced amino acid secretion in Arabidopsis. *Plant Physiology*, 158, 1628–1642.

Pratelli, R., Voll, L.M., Horst, R.J., Frommer, W.B. & Pilot, G. (2010) Stimulation of nonselective amino acid export by glutamine dumper proteins. *Plant Physiology*, 152, 762–773.

Price, A.J., Hwang, T., Tao, R., Burke, E.E., Rajpurohit, A., Shin, J.H. et al. (2020) Characterizing the nuclear and cytoplasmic transcriptomes in developing and mature human cortex uncovers new insight into psychiatric disease gene regulation. *Genome Research*, 30, 1–11.

Rabani, M., Raychowdhury, R., Jovanovic, M., Rooney, M., Stumpo, D., Pauli, A. et al. (2014) High resolution sequencing and modeling identifies distinct dynamic RNA regulatory strategies. *Cell*, 159, 1698–1710.

Rahayu, Y.S., Walch-Liu, P., Neumann, G., Römheld, V., von Wirén, N. & Bangerth, F. (2005) Root-derived cytokinins as long-distance signals for NO3--induced stimulation of leaf growth. *Journal of Experimental Botany*, 56, 1143–1152.

Ramakers, C., Timmer, D., Bakker, O., Deprez, R.H.L., Ruijter, J.M. & Moorman, A.F.M. (2004) Quantification of mRNA USING LINEAR REGRESSION OF LOG-LINEAR PCR DATA-POINTS AS AN ALTERNATIVE FOR THE STANDARD CURVE APPROACH. In: Wittwer, C., Hahn, M. & Kaul, K. (Eds.) *Rapid cycle real-time PCR—Methods and applications: Quantification*. Springer, pp. 21–29.

Remans, T., Keunen, E., Bex, G.J., Smeets, K., Vangronsveld, J. & Cuypers, A. (2014) Reliable gene expression analysis by reverse transcription-quantitative PCR: reporting and minimizing the uncertainty in data accuracy. *The Plant Cell*, 26, 3829–3837.

Reynoso, M.A., Kajala, K., Bajic, M., West, D.A., Pauluzzi, G., Yao, A.I. et al. (2019) Evolutionary flexibility in flooding response circuitry in angiosperms. *Science*, 365, 1291–1295.

Riveras, E., Alvarez, J.M., Vidal, E.A., Oses, C., Vega, A. & Gutiérrez, R.A. (2015) The calcium ion is a second messenger in the nitrate signaling pathway of Arabidopsis. *Plant Physiology*, 169, 1397–1404.

Rosa, S., Duncan, S. & Dean, C. (2016) Mutually exclusive sense-antisense transcription at FLC facilitates environmentally induced gene repression. *Nature Communications*, 7, 13031.

Ruffel, S., Krouk, G., Ristova, D., Shasha, D., Birnbaum, K.D. & Coruzzi, G.M. (2011) Nitrogen economics of root foraging: transitive closure of the nitrate – cytokinin relay and distinct systemic signaling for N supply vs. demand. *Proceedings of the National Academy of Sciences*, 108, 18524–18529.

Saavedra, C., Tung, K.S., Amberg, D.C., Hopper, A.K. & Cole, C.N. (1996) Regulation of mRNA export in response to stress in Saccharomyces cerevisiae. *Genes & Development*, 10, 1608–1620. Available from: https://doi.org/10.1101/gad.10.13.1608

Saeed, A.I., Sharov, V., White, J., Li, J., Liang, W., Bhagabati, N. et al. (2003) TM4: a free, open-source system for microarray data management and analysis. *Biotechniques*, 34, 374–378.

Saleh, A., Alvarez-Venegas, R. & Avramova, Z. (2008) An efficient chromatin immunoprecipitation (ChIP) protocol for studying histone modifications in Arabidopsis plants. *Nature Protocols*, 3, 1018–1025.

Santos-Filho, P.R., Saviani, E.E., Salgado, I. & Oliveira, H.C. (2014) The effect of nitrate assimilation deficiency on the carbon and nitrogen status of *Arabidopsis thaliana* plants. *Amino Acids*, 46, 1121–1129.

Schaffner, W. (1988) A hit-and-run mechanism for transcriptional activation? *Nature*, 336, 427–428.

Scheible, W.-R., Gonzalez-Fontes, A., Lauerer, M., Muller-Rober, B., Caboche, M. & Stitt, M. (1997) Nitrate acts as a signal to induce organic acid metabolism and repress starch metabolism in tobacco. *The Plant Cell*, 9, 783–798.

Schwanhäusser, B., Busse, D., Li, N., Dittmar, G., Schuchhardt, J., Wolf, J. et al. (2011) Global quantification of mammalian gene expression control. *Nature*, 473, 337–342.

Smyth, G.K. (2005) Limma: linear models for microarray data. In: Gentleman, R., Carey, V.J., Huber, W., Irizarry, R.A. & Dudoit, S. (Eds.) *Bioinformatics and computational biology solutions using R and Bioconductor* (pp. 397–420), 1st ed. Springer.

Solnestam, B.W., Stranneheim, H., Hällman, J., Käller, M., Lundberg, E., Lundeberg, J. et al. (2012) Comparison of total and cytoplasmic mRNA reveals global regulation by nuclear retention and miRNAs. *BMC Genomics*, 13, 574.

Soneson, C., Love, M.I. & Robinson, M.D. (2016) Differential analyses for RNA-seq: transcript-level estimates improve gene-level inferences. *F1000Research*, 4, 1521.

Sorenson, R.S., Deshotel, M.J., Johnson, K., Adler, F.R. & Sieburth, L.E. (2018) Arabidopsis mRNA decay landscape arises from specialized RNA decay substrates, decapping-mediated feedback, and redundancy. *Proceedings of the National Academy of Sciences*, 115, 1485–1494.

Stirling, D.R., Swain-Bowden, M.J., Lucas, A.M., Carpenter, A.E., Cimini, B.A. & Goodman, A. (2021) CellProfiler 4: improvements in speed, utility and usability. *BMC Bioinformatics*, 22, 433.

Sun, M., Schwalb, B., Schulz, D., Pirkl, N., Etzold, S., Larivière, L. et al. (2012) Comparative dynamic transcriptome analysis (cDTA) reveals mutual feedback between mRNA synthesis and degradation. *Genome Research*, 22, 1350–1359.

Supek, F., Bošnjak, M., Škunca, N. & Šmuc, T. (2011) REVIGO summarizes and visualizes long lists of gene ontology terms. *PLoS One*, 6, e21800.

Swift, J., Alvarez, J.M., Araus, V., Gutiérrez, R.A. & Coruzzi, G.M. (2020) Nutrient dose-responsive transcriptome changes driven by Michaelis – Menten kinetics underlie plant growth rates. *Proceedings of the National Academy of Sciences*, 117, 12531–12540.

Szabo, E.X., Reichert, P., Lehniger, M.K., Ohmer, M., de Francisco Amorim, M., Gowik, U. et al. (2020) Metabolic labeling of RNAs uncovers hidden features and dynamics of the Arabidopsis transcriptome. *The Plant Cell*, 32, 871–887.

Tang, X., Peng, Y., Li, Z., Guo, H., Xia, X., Li, B. et al. (2022) The regulation of nitrate reductases in response to abiotic stress in Arabidopsis. *International Journal of Molecular Sciences*, 23, 1202.

Thieme, C.J., Rojas-Triana, M., Stecyk, E., Schudoma, C., Zhang, W., Yang, L. et al. (2015) Endogenous Arabidopsis messenger RNAs transported to distant tissues. *Nature Plants*, 1, 15025.

Tippmann, S.C., Ivanek, R., Gaidatzis, D., Schöler, A., Hoerner, L. & Van Nimwegen, E. et al. (2012) Chromatin measurements reveal contributions of synthesis and decay to steady-state mRNA levels. *Molecular Systems Biology*, 8, 593.

Tudek, A., Schmid, M. & Jensen, T.H. (2019) Escaping nuclear decay: the significance of mRNA export for gene expression. *Current Genetics*, 65, 473–476.

Undurraga, S.F., Ibarra-Henríquez, C., Fredes, I., Álvarez, J.M. & Gutiérrez, R.A. (2017) Nitrate signaling and early responses in Arabidopsis roots. *Journal of Experimental Botany*, 68, 2541–2551.

Varala, K., Marshall-Colón, A., Cirrone, J., Brooks, M.D., Pasquino, A.V., Léran, S. et al. (2018) Temporal transcriptional logic of dynamic regulatory networks underlying nitrogen signaling and use in plants. *Proceedings of the National Academy of Sciences*, 115, 6494–6499.

Vidal, E.A., Alvarez, J.M., Araus, V., Riveras, E., Brooks, M.D., Krouk, G. et al. (2020) Nitrate in 2020: thirty years from transport to signaling networks. *The Plant Cell*, 32, 2094–2119.

Vidal, E.A., Araus, V., Lu, C., Parry, G., Green, P.J., Coruzzi, G.M. et al. (2010) Nitrate-responsive miR393/AFB3 regulatory module controls root system architecture in *Arabidopsis thaliana*. *Proceedings of the National Academy of Sciences*, 107, 4477–4482.

Vidal, E.A., Moyano, T.C., Krouk, G., Katari, M.S., Tanurdzic, M., McCombie, W.R. et al. (2013) Integrated RNA-seq and sRNA-seq analysis identifies novel nitrate-responsive genes in *Arabidopsis thaliana* roots. *BMC Genomics*, 14, 701.

Walker, L., Boddington, C., Jenkins, D., Wang, Y., Grønlund, J.T., Hulsmans, J. et al. (2017) Changes in gene expression in space and time orchestrate environmentally mediated shaping of root architecture. *The Plant Cell*, 29, 2393–2412.

Wang, R., Okamoto, M., Xing, X. & Crawford, N.M. (2003) Microarray analysis of the nitrate response in Arabidopsis roots and shoots reveals over 1,000 rapidly responding genes and new linkages to glucose, trehalose-6-phosphate, iron, and sulfate metabolism. *Plant Physiology*, 132, 556–567.

Wang, R., Tischner, R., Gutiérrez, R.A., Hoffman, M., Xing, X., Chen, M. et al. (2004) Genomic analysis of the nitrate response using a nitrate reductase-null mutant of Arabidopsis. *Plant Physiology*, 136, 2512–2522.

Wang, R., Xing, X. & Crawford, N. (2007) Nitrite acts as a transcriptome signal at micromolar concentrations in Arabidopsis roots. *Plant Physiology*, 145, 1735–1745.

Wickramasinghe, V.O. & Laskey, R.A. (2015) Control of mammalian gene expression by selective mRNA export. *Nature Reviews Molecular Cell Biology*, 16, 431–442.

Wu, H., Li, B., Iwakawa, H.o, Pan, Y., Tang, X., Ling-hu, Q. et al. (2020) Plant 22-nt siRNAs mediate translational repression and stress adaptation. *Nature*, 581, 89–93.

Xiao, H., Hu, Y., Wang, Y., Cheng, J. & Chen, G. (2022) Nitrate availability controls translocation of the transcription factor NAC075 for cell-type-specific reprogramming of root growth. *Developmental Cell*, 57(23), 2638–2651. Available from: https://doi.org/10.1016/j.devcel.2022.11.006

Xu, F. & Copeland, C. (2012) Nuclear extraction from *Arabidopsis thaliana*. *Bio-protocol*, 2, 18–21.

Yan, D., Easwaran, V., Chau, V., Okamoto, M., Ierullo, M., Kimura, M. et al. (2016) NIN-like protein 8 is a master regulator of nitrate-promoted seed germination in Arabidopsis. *Nature Communications*, 7, 13179.

Yang, W., Wightman, R. & Meyerowitz, E.M. (2017) Cell cycle control by nuclear sequestration of CDC20 and CDH1 mRNA in plant stem cells. *Mol.Cell*, 68, 1108–1119.

Yeap, W.-C., Namasivayam, P., Ooi, T.E.K., Appleton, D.R., Kulaveerasingam, H. & Ho, C. (2019) EgRBP42 from oil palm enhances adaptation to stress in Arabidopsis through regulation of nucleocytoplasmic transport of stress-responsive mRNAs. *Plant, Cell & Environment*, 42, 1657–1673.

Yelina, N.E., Smith, L.M., Jones, A.M.E., Patel, K., Kelly, K.A. & Baulcombe, D.C. (2010) Putative Arabidopsis THO/TREX mRNA export complex is involved in transgene and endogenous siRNA biosynthesis. *Proceedings of the National Academy of Sciences*, 107, 13948–13953.

Yu, S., Pratelli, R., Denbow, C. & Pilot, G. (2015) Suppressor mutations in the Glutamine Dumper1 protein dissociate disturbance in amino acid transport from other characteristics of the Gdu1D phenotype. *Frontiers in Plant Science*, 6, 149734.

Zander, G., Hackmann, A., Bender, L., Becker, D. & Salinas, G. (2016) mRNA quality control is bypassed for immediate export of stress-responsive transcripts nature letters. *Nature Publishing Group*, 540, 593–596. https://doi.org/10.1038/nature20572

Zhao, L., Liu, F., Crawford, N.M. & Wang, Y. (2018) Molecular regulation of nitrate responses in plants. *International Journal of Molecular Sciences*, 19, 2039.

Zhao, R.R., Qu, B.Y., Tong, Y.P. & Zou, C.Q. (2019) Iron and zinc accumulation in winter wheat regulated by NICOTIANAMINE SYNTHASE responded to increasing nitrogen levels. *Journal of Plant Nutrition*, 42, 1624–1636.

SUPPORTING INFORMATION

Additional supporting information can be found online in the Supporting Information section at the end of this article.

How to cite this article: Fonseca, A., Riveras, E., Moyano, T.C., Alvarez, J.M., Rosa, S. & Gutiérrez, R.A. (2024) Dynamic changes in mRNA nucleocytoplasmic localization in the nitrate response of Arabidopsis roots. *Plant, Cell & Environment*, 47, 4227–4245. https://doi.org/10.1111/pce.15018